IVYSPRING INTERNATIONAL PUBLISHER

Theranostics

2018; 8(16): 4372-4392. doi: 10.7150/thno.27088

Research Paper

3D printing of Mo-containing scaffolds with activated anabolic responses and bi-lineage bioactivities

Wentao Dang[1,2], Xiaoya Wang[1], Jiayi Li[3], Cuijun Deng[1,2], Yaqin Liu[1,2], Qingqiang Yao[3], Liming Wang[3], Jiang Chang[1], Chengtie Wu[1]✉

1. State Key Laboratory of High Performance Ceramics and Superfine Microstructure, Shanghai Institute of Ceramics, Chinese Academy of Sciences, Shanghai 200050, People's Republic of China.
2. University of Chinese academy of Sciences, Beijing, People's Republic of China
3. Department of Orthopaedic Surgery Digital Medicine Institute, Nanjing Medical University, Nanjing Hospital. No. 68 Changle Road Nanjing, 210006, People's Republic of China

W. Dang and X.Wang are the co-first authors.

✉ Corresponding author: E-mail: chengtiewu@mail.sic.ac.cn (C. Wu)

Received: 2018.05.05; Accepted: 2018.06.30; Published: 2018.07.30

Abstract

When osteochondral tissues suffer from focal or degenerative lesions caused by trauma or disorders, it is a tough challenge to regenerate them because of the limited self-healing capacity of articular cartilage. In this study, a series of Mo-doped bioactive glass ceramic (Mo-BGC) scaffolds were prepared and then systematically characterized. The released MoO_4^{2-} ions from 7.5Mo-BGC scaffolds played a vital role in regenerating articular cartilage and subchondral bone synchronously.

Methods: The Mo-BGC scaffolds were fabricated through employing both a sol-gel method and 3D printing technology. SEM, EDS, HRTEM, XRD, ICPAES and mechanical strength tests were respectively applied to analyze the physicochemical properties of Mo-BGC scaffolds. The proliferation and differentiation of rabbit chondrocytes (RCs) and human bone mesenchymal stem cells (HBMSCs) cultured with dilute solutions of 7.5Mo-BGC powder extract were investigated *in vitro*. The co-culture model was established to explore the possible mechanism of stimulatory effects of MoO_4^{2-} ions on the RCs and HBMSCs. The efficacy of regenerating articular cartilage and subchondral bone using 7.5Mo-BGC scaffolds was evaluated *in vivo*.

Results: The incorporation of Mo into BGC scaffolds effectively enhanced the compressive strength of scaffolds owing to the improved surface densification. The MoO_4^{2-} ions released from the 7.5Mo-BGC powders remarkably promoted the proliferation and differentiation of both RCs and HBMSCs. The MoO_4^{2-} ions in the co-culture system significantly stimulated the chondrogenic differentiation of RCs and meanwhile induced the chondrogenesis of HBMSCs. The chondrogenesis stimulated by MoO_4^{2-} ions happened through two pathways: 1) MoO_4^{2-} ions elicited anabolic responses through activating the HIF-1α signaling pathway; 2) MoO_4^{2-} ions inhibited catabolic responses and protected cartilage matrix from degradation. The *in vivo* study showed that 7.5Mo-BGC scaffolds were able to significantly promote cartilage/bone regeneration when implanted into rabbit osteochondral defects for 8 and 12 weeks, displaying bi-lineage bioactivities.

Conclusion: The 3D-printed Mo-BGC scaffolds with bi-lineage bioactivities and activated anabolic responses could offer an effective strategy for cartilage/bone interface regeneration.

Introduction

Osteochondral tissues are mainly comprised of two distinct compartments, namely articular cartilage and underlying subchondral bone [1, 2]. The articular cartilage is primarily composed of chondrocytes and extracellular matrix (ECM) that mainly contains water, collagen type II, and proteoglycans such as aggrecan [3-5]. When articular cartilage suffers focal or degenerative lesions caused by trauma or disorders, it has a limited capacity for self-healing because of its avascularity and low cellularity and ultimately could evolve into osteoarthritis (OA) that in turn could result in the degradation of articular

hyaline cartilage and subchondral bone structural remodeling [6-12]. Thus, it is extremely significant to repair osteochondral defects and acquire new cartilage and bone tissues. Currently, bone marrow stimulation techniques such as microfracture and drilling methods as well as autologous chondrocyte implantation are useful treatments. However, they have respective shortcomings. The bone marrow stimulation techniques cannot fully remedy the osteochondral defect and may inflict further tissue damage. The autologous chondrocyte implantation has problems of donor-site morbidity and disturbed remodeling of the osteochondral unit [13-15]. Additionally, the density of chondrocytes used for autologous implantation is relatively low in the native articular cartilage. The *in vitro* expansion and culture of chondrocytes can lead to undesirable changes in chondrocyte phenotype [16, 17]. The ideal therapeutic strategy for osteochondral defects is that the treatment can simultaneously regenerate the articular cartilage and subchondral bone. Scaffolds are an integral part of bone tissue engineering and the scaffolds employed for bone tissue engineering should have good biocompatibility, biodegradability, mechanical properties as well as interconnected pore structure with high porosity to guarantee cellular penetration and adequate diffusion of nutrients to cells [18-23]. In past years, some biphasic, triphasic, and multilayered gradient scaffolds with specifically designed scaffold-cell constructs have been fabricated to repair osteochondral defects through simulating the physiological microstructure of articular cartilage and subchondral bone. However, they are unable to completely mimic the biological construction and properties of cartilage and subchondral bone owing to the complex interface of the osteochondral tissues. In addition, the mechanical stability between two phases of the biphasic scaffold is questionable and the multiphasic structures are too complex to control the properties of each phase such as their degradation behavior and shear forces between the phases [24-28]. Therefore, preparing a single kind of scaffold with dual bioactivities that could simultaneously regenerate both cartilage and subchondral bone is highly desired.

Molybdenum (Mo) is an essential trace element for plants, animals and microorganisms. When Mo enters organisms, it can make up several Mo-enzymes such as aldehyde oxidase (AO), xanthine oxidase (XO), sulfite oxidase (SO), and nitrate reductase (NR). These Mo-enzymes are involved in various biochemical reactions through combining with respective substrates and play important roles in physiology [29-33]. In recent years, some metal alloys containing Mo such as Co-Cr-Mo have been found to possess excellent mechanical properties and good biocompatibility, and have been widely used as orthopedic and dental implants [34-36]. Kanaji *et al.* showed that Mo ions did not result in cell death under 0.5 mM (48 ppm) and could promote the proliferation of MLO-Y4 osteocytes at 0.5 mM [37], which indicated that Mo ions may own great potential for biological applications such as bone tissue engineering. To our best knowledge, there are no reported studies about the influences of Mo on chondrogenesis and osteogenesis of RCs and HBMSCs. Additionally, a study applying Mo to repairing osteochondral defect has not been reported. We hypothesized that Mo-containing scaffolds may have dual bioactivities for cartilage/bone regeneration in osteochondral defects. Therefore, in this study, Mo-BGC scaffolds were successfully prepared using both a sol-gel method and 3D printing technique. The capacity of 7.5Mo-BGC scaffolds for repairing osteochondral defects and the corresponding mechanism for stimulating osteochondral regeneration were systematically investigated, as shown in **Graphical abstract.**

Methods

Materials

Tetraethyl orthosilicate ($(C_2H_5O)_4Si$, TEOS), triethyl phosphate ($(C_2H_5O)_3PO$, TEP), calcium nitrate tetrahydrate ($Ca(NO_3)_2{\cdot}4H_2O$) and ammonium molybdate tetrahydrate ($(NH_4)_6Mo_7O_{24}{\cdot}4H_2O$) were purchased from Sinopharm Chemical Reagent Co., Ltd. (China). Ammonium molybdate ($(NH_4)_2MoO_4$) was purchased from Macklin biochemical technology Co., Ltd. (China). Pluronic F-127 was purchased from Sigma-Aldrich (USA).

Synthesis of Mo-BGC powders through sol-gel method

BGC and Mo-BGC powders were synthesized through a sol-gel method. The detailed procedures were as follows. Firstly, 157 mL of TEOS and 25 mL of HNO_3 (2 M) were successively added to 200 mL of deionized water, then stirred constantly by a magnetic stirring apparatus for 30 min. After sufficient hydrolysis, $Ca(NO_3)_2{\cdot}4H_2O$ (59.00 g, 54.31 g, 47.23 g, 41.30 g), $(NH_4)_6Mo_7O_{24}{\cdot}4H_2O$ (0 g, 3.53 g, 8.83 g, 13.24 g) and 8.53 mL of TEP were then added into the TEOS solution at molar ratios of 70:25:5:0, 70:23:5:2, 70:20:5:5 and 70:17.5:5:7.5 (Si:Ca:P:Mo) for further reaction to obtain four different solutions. After 5 h, these solutions were transferred to an air oven and maintained for 48 h at 60 °C to generate wet gels. Then, these wet gels were dried in an 120 °C air oven for 24 h. The dried bioactive glass gel abbreviated as

$Ca_{25}Si_{70}P_5O_{177.5}$ and Mo-doped bioactive glass gel abbreviated as $Ca_{25-x}Si_{70}P_5Mo_xO_{177.5+2x}$ (x=2, 5, 7.5) were milled for 5 h at a speed of 500 rpm through a planetary high-energy ball mill and the ground powders were then calcined by an energy-save-type electric furnace (SSJ-14, China) for 3 h at 800 °C and then filtered by a 300 mesh sifter to obtain final BGC and Mo-BGC powders.

Preparation of Mo-BGC scaffolds through 3D printing

The printable glass ceramic ink was prepared by mixing 5 g of (2, 5, 7.5)Mo-BGC powders with 3.5 g of pluronic F-127 (20 wt%) aqueous solution. After being stirred to homogeneity, the ink was transferred into a tube and printed by a needle (standard: 22 G) through a 3D plotting device that was designed by the Fraunhofer Institute for Materials Research and Beam Technology (Dresden, Germany). The dosing pressure was 1.5-3.0 bar and the printing speed was 5 mm/s. The printing was conducted at room temperature. The printed wet scaffolds were dried overnight at room temperature and subsequently sintered at 1350 °C for 3 h at a heating rate of 2 °C/min in a Nabertherm industrial furnace (LH 15/14, Germany) to obtain the final scaffolds. BGC scaffolds were fabricated by the same method as the control.

Characterization of Mo-BGC scaffolds

Macroscopic photographs of BGC and (2, 5, 7.5)Mo-BGC scaffolds were taken using a camera (Nikon). The overall microscopic images of BGC and (2, 5, 7.5)Mo-BGC scaffolds were acquired by optical microscopy (S6D, Leica, Germany). The surface morphology and elemental distribution of BGC and (2, 5, 7.5)Mo-BGC scaffolds were characterized using a scanning electron microscope (SEM, SU8220, HITACHI, Japan) equipped with an energy dispersive spectrometer (EDS). The phase compositions of BGC, (2, 5, 7.5)Mo-BGC powders and scaffolds were tested by a X-ray diffractometer using Cu Kα radiation (XRD, D8 ADVANCE, BRUKER AXS GMBH, Germany). The phase compositions of 5Mo-BGC were checked by high-resolution transmission electron microscopy (HRTEM, JEM-2100F, Japan). The elemental contents of BGC and (2, 5, 7.5)Mo-BGC scaffolds were measured by inductively coupled plasma-atomic emission spectrometry (ICP-AES, Vista AX, Varian, US).

Mechanical strength and degradation behavior of Mo-BGC scaffolds

The compressive strengths of BGC and (2, 5, 7.5)Mo-BGC scaffolds (diameter: 8 mm; height: 9 mm) were tested by a computer-controlled universal testing machine (AG-I, Shimadzu, Japan) with a cross-head speed of 0.5 mm/min (n=5 for each group). Representative photographs of BGC and (2, 5, 7.5)Mo-BGC scaffolds used for compressive strength tests are shown in **Figure S1**. To assess the degradation behavior of BGC (control group) and (2, 5, 7.5)Mo-BGC scaffolds, tris-HCl solution (pH=7.4) was added to BGC and (2, 5, 7.5)Mo-BGC scaffolds at a ratio of 200 mL/g (tris-HCl solution volume/scaffold mass) in 50 mL test tubes (n=3 for each group). Then, these test tubes were put into a shaker for 3, 7, 14, 21, and 28 days at 37 °C. After each shaking time, the scaffolds were taken from the tris-HCl solution and dried in a 60 °C air oven, and the final weight of each scaffold was measured. The weight loss of the scaffolds was expressed as the ratio of the final weight to the initial weight. In addition, the tris-HCl solutions at each time point were collected and the concentrations of released Mo, Ca, Si, P in solutions were measured by ICP-AES.

In vitro proliferation and differentiation of RCs and HBMSCs cultivated with dilute solutions of 7.5Mo-BGC powder extract

The proliferations of RCs and HBMSCs cultivated with dilute solutions of BGC (control group) and 7.5Mo-BGC powder extracts (200 mg/mL) were tested by CCK8 assay (cell counting kit-8, Beyotime, China). Firstly, both RCs and HBMSCs were respectively incubated with dilute solutions in a 96-well plate (Thermo Fisher Scientific) for 1, 3 and 7 days (1000 cells/well, 100 μL/well). Afterwards, RCs and HBMSCs were incubated with 10% CCK8 solution in an incubator with 5% CO_2 for 1.5 h at 37 °C. Finally, the absorbance value of culture medium was measured at 450 nm by a multifunction microplate reader (SpectraFluor Plus, Tecan, Crailsheim, Germany). The dilute solutions of BGC and 7.5Mo-BGC powder extracts (200 mg/mL) were prepared as follows. Firstly, 2.0 g BGC or 7.5Mo-BGC powders were added to 10 mL Dulbecco's modified Eagle's medium (DMEM, Gibco) or HBMSCs basal medium (Cyagen) and then vibrated for 24 h at 37 °C at a rotation speed of 120 r/min. Subsequently, the extract was centrifuged and filtered by a 0.22 μm filter. Finally, the filtered extract (set as 1) was diluted 1/2, 1/4, 1/8, 1/16, 1/32, 1/64, 1/128 in DMEM or HBMSCs basal medium. The concentrations of Ca, Si, P, Mo elements in the BGC and 7.5Mo-BGC powder extracts (200 mg/mL) along with their dilute solutions (1/2, 1/8, 1/64 groups) were analyzed by ICP-AES. The results are shown in **Table S2**.

Real-time polymerase chain reaction (PCR) assay was conducted to study the effects of dilute solutions of BGC and 7.5Mo-BGC powder extracts on

chondrogenic and osteogenic differentiation-related genes. In brief, both RCs and HBMSCs were respectively incubated with dilute solutions (1/2, 1/8, 1/64 groups) of BGC and 7.5Mo-BGC powder extracts in a 6-well plate (Thermo Fisher Scientific) for 7 days (200000 cells/well, 2.5 mL/well). Then these RCs and HBMSCs were processed by a trizol reagent (Invitrogen) for total RNA extraction to evaluate the mRNA transcript levels of chondrogenic differentiation-related genes (COL II, ACAN, SOX9 and N-cadh) and osteogenic differentiation-related genes (COL I, OCN, BMP2, and RUNX2). The RNA concentration was obtained by a multifunction microplate reader (SpectraFluor Plus, Tecan, Crailsheim, Germany) at 260 nm. The relative expression level of each target gene was calculated by the ΔCt method. The sequences of genes used for real-time PCR are shown in **Table S3**.

ALP and alizarin red stainings of HBMSCs cultivated with dilute solutions of 7.5Mo-BGC powder extract

Alkaline phosphatase (ALP) staining was conducted using an ALP histochemical diagnostic kit (Beyotime, China). Firstly, HBMSCs were respectively cultured with dilute solutions (1/2, 1/8, 1/64 groups) of BGC (control group) and 7.5Mo-BGC powder extracts in a 6-well plate (Thermo Fisher Scientific) for 7 days (200000 cells/well, 2.5 mL/well), then these HBMSCs were fixed with 4% paraformaldehyde (Sinopharm Chemical Reagent Co., Ltd, China), then incubated with a mixture of fast blue B salt and Naphthol AS-MX phosphate. Lastly, HBMSCs were rinsed in deionized water, then observed and photographed by a light microscope (X7; Olympus, Tokyo, Japan). To identify the formation of calcium nodules in HBMSCs cultured with dilute solutions of BGC and 7.5Mo-BGC powder extracts, alizarin red staining was conducted. In brief, after culturing with dilute solutions (1/2, 1/8, 1/64 groups) of BGC and 7.5Mo-BGC powder extracts in 6-well plates (Thermo Fisher Scientific) for 7 days (200000 cells/well, 2.5 mL/well), the HBMSCs were incubated with alizarin red solution (Cyagen Biosciences, America) at room temperature for 5 min. Subsequently, cells were washed thrice with DPBS to remove excess staining solution. The calcium nodules were stained as red spots and photographed by a light microscope (X7; Olympus, Tokyo, Japan).

In vitro proliferation and attachment of RCs and HBMSCs on Mo-BGC scaffolds

Both BGC (control group) and Mo-BGC scaffolds were sterilized by steam. Then, RCs and HBMSCs were cultured with BGC and Mo-BGC scaffolds in 48-well plates (Thermo Fisher Scientific) for 1, 3, 7 days (5000 cells/well, 0.5 mL/well). Subsequently, the RCs and HBMSCs were incubated with 10% CCK8 solution in an incubator with 5% CO_2 for 1.5 h at 37 °C, and the OD value was measured at 450 nm. Moreover, to observe the morphology and adhesion of cells on BGC and 7.5Mo-BGC scaffolds, RCs and HBMSCs were cultured with BGC and 7.5Mo-BGC scaffolds for 1 and 7 days. Then, the culture medium was removed and scaffolds were fixed with 2.5% glutaraldehyde for 20 min, washed with deionized water three times, and then dehydrated in graded ethanol (30%, 50%, 70%, 80%, 90%, 95%, and 100%) and hexamethyldisilizane (HMDS) in sequence. Finally, the dehydrated cellular scaffolds were coated with gold and observed by SEM (SU8220, HITACHI, Japan). Meanwhile, the cytoskeleton and cell nuclei were stained by fluorescein isothiocyanate phalloidin (Sigma-Aldrich, USA) and DAPI (Sigma-Aldrich, USA), respectively. Then the morphology of RCs and HBMSCs cultured on BGC and 7.5Mo-BGC scaffolds was observed by CLSM (Leica TCS SP8).

Effects of MoO_4^{2-} ions on chondrogenic differentiation of RCs and HBMSCs in a co-culture system

An *in vitro* co-culture model of RCs, HBMSCs and MoO_4^{2-} ions was established to explore the effect of MoO_4^{2-} ions on chondrogenic differentiation. Firstly, HBMSCs were seeded onto the lower chambers of a 6-well plate (Thermo Fisher Scientific) and RCs were seeded onto Mllicell hanging cell culture inserts (0.4 μm pore size; Millipore, Billerica, MA, USA). The RCs and HBMSCs were respectively seeded onto the insert and well at a ratio of 1:1 (200000 cells). The growth medium consisted of low-glucose DMEM, 10% FBS, and 1% penicillin-streptomycin. After the co-culture system was maintained in an incubator with 5% CO_2 at 37 °C for 24 h, the co-culture medium was replaced by growth medium containing different concentrations of MoO_4^{2-} ions (2, 6, 10 mg/L of Mo), with the co-culture of RCs and HBMSCs without MoO_4^{2-} ions (0 mg/L) as control group. After 3 days, cells were collected and total RNAs of HIF-1a, HIF-2a, SOX9, COL II, ACAN, TIMP3, MMP13 and ADAMTS5 from the co-cultured cells were extracted for real-time PCR assay. The sequences of gene used for real-time PCR are shown in **Table S3**.

In vivo repair of osteochondral defects by 7.5Mo-BGC scaffolds

The animal experimental protocol used in this study was approved by the Nanjing Medical University Ethics Committee. Twenty-eight New Zealand white rabbits (2.5-3.0 kg, 6 months) were

chosen as models for evaluating the efficacy of repairing osteochondral defects of BGC (control group) and 7.5Mo-BGC scaffolds. Two osteochondral cylindrical cartilage defects were created (diameter: 4 mm, height: 5 mm) in the patellar groove, then BGC or 7.5Mo-BGC scaffolds were implanted into these defects, respectively. The untreated defects were the blank group (n=7 for each group). After 8 or 12 weeks, rabbits were sacrificed and seven knee joint specimens from each group were collected. The collected specimens from each group were photographed for evaluating the regeneration efficacy of articular cartilage in accordance with the ICRS macroscopic assessment scale for cartilage repair [38]. Additionally, a micro-CT scanner (Bruker, Germany) was used to acquire 3D reconstruction images and analyze the new cartilage and bone tissue formation. After photographing and micro-CT analysis, six sections from each specimen were stained with safranin O and alizarin red to further evaluate the regeneration efficacy of articular cartilage and subchondral bone.

Statistical analysis

All data are expressed as mean ± standard deviation (SD) and were analyzed using one-way ANOVA statistical analysis to evaluate the significance of the experimental data. *P < 0.05, **P < 0.01, ***P < 0.001.

Results

The $CaMoO_4$ phase formed during the calcining process of Mo-BGC powders at 800 °C and improved compressive strength of the scaffolds through enhancing the surface densification of scaffolds. The *in vitro* experiment demonstrated that 1/8 dilute solution of 7.5Mo-BGC powder extract significantly promoted chondrogenic differentiation of RCs and osteogenic differentiation of HBMSCs respectively as compared to BGC. The *in vivo* animal experiment showed that 7.5Mo-BGC scaffolds promoted cartilage/bone regeneration simultaneously better than BGC. The mechanism investigation indicated that The MoO_4^{2-} ions in the co-culture system significantly stimulated the chondrogenic differentiation of RCs and meanwhile induced the chondrogenesis of HBMSCs.

Characterization of Mo-BGC scaffolds

Photographs of four kinds of scaffolds (BGC, 2Mo-BGC, 5Mo-BGC and 7.5Mo-BGC scaffolds) are shown in **Figure 1A**. It could be seen that the color of all the scaffolds was white and their macroscopic appearances did not exhibit obvious differences (**Figure 1B**). The shape of these scaffolds was cylindrical with an approximate diameter of 8 mm and height of 2 mm. However, the microstructure of these scaffolds was very distinct. Different sizes of micropores were distributed on the strut walls of the BGC scaffold, while these micropores disappeared in the Mo-BGC scaffolds.

Figure 1M-N shows the XRD patterns of BGC and (2, 5, 7.5)Mo-BGC powders calcined at 800 °C (M) and sintered at 1350 °C (N). Some broad peaks appeared at 23° according to the XRD patterns of the BGC and (2, 5, 7.5)Mo-BGC powders, indicating that some amorphous phases existed in the synthesized powders. The BGC powders mainly consisted of $CaSiO_3$ and $Ca_{10}(PO_4)_6(OH)_2$ phases. Also, the $CaMoO_4$ phase could be detected in the (2, 5, 7.5)Mo-BGC powders in addition to $CaSiO_3$ and $Ca_{10}(PO_4)_6(OH)_2$ phases, indicating that $CaMoO_4$ could form at the calcining process of (2, 5, 7.5)Mo-BGC powders at 800 °C. The diffraction peak of the amorphous phase vanished after sintering at 1350 °C and new SiO_2 phases appeared in the BGC and (2, 5, 7.5)Mo-BGC scaffolds. In addition, the $Ca_{10}(PO_4)_6(OH)_2$ phase transformed to $Ca_3(PO_4)_2$ phase at 1350 °C. The diffraction peaks of $CaMoO_4$ were indexed to the tetragonal phase with the cell parameters a=5.226 Å, b=5.226 Å and c=11.430 Å (ICDD/JCPDS Card No. 29-0351). Because of its low melting point (965 °C), the $CaMoO_4$ phase melted during the sintering process at 1350 °C, which thus could enhance the surface density of Mo-BGC scaffolds.

In order to further check the phase compositions of Mo-BGC scaffolds, EDS analysis for element mapping was conducted (**Figure 2A**). The $CaMoO_4$, SiO_2, and $CaSiO_3$ crystal phases in 5Mo-BGC scaffold could be clearly identified owing to the strong signal intensities of Ca, Si and Mo elements, while the signal intensity of P element was relatively weak. In addition, selected area electron diffraction (SAED), high-resolution transmission electron microscopy (HRTEM) and energy dispersive spectrometry (EDS) were performed to analyze randomly chosen fragments from 5Mo-BGC scaffold. **Figure 2B** shows the SAED, HRTEM and EDS results of $CaMoO_4$. Some ordered and sharp diffraction spots of $CaMoO_4$ crystal (**Figure 2B$_1$**) were acquired, which indicated that $CaMoO_4$ exists in the Mo-BGC scaffolds in the form of a monocrystal. The SAED pattern of $CaMoO_4$ monocrystal was indexed to a tetragonal scheelite structure. **Figure 2B$_2$** shows the HRTEM image of $CaMoO_4$ monocrystal with an interplanar spacing of 0.198 nm corresponding to the crystal face (213) of $CaMoO_4$. The detected atomic percentages of Ca, Mo and O elements in $CaMoO_4$ were 11.36±0.97%, 15.37±0.96% and 72.67±1.87%, respectively. **Figure**

2C-D show the SAED, HRTEM and EDS results of the SiO_2, and $CaSiO_3$ phases. The diffraction spots of monocrystal SiO_2 were well acquired according to the SAED (**Figure 2C$_1$**), while it was interesting that the interplanar spacing of the SiO_2 phase could not be well identified by HRTEM (**Figure 2C$_2$**). A possible reason is that the crystal structure of monocrystal SiO_2 was destroyed due to the high-energy electron beam. In addition, the diffraction spots, interplanar spacing of the crystal face (117) and detected atomic percentages of Ca, Si and O elements of $CaSiO_3$ monocrystal are shown in **Figure 2D**.

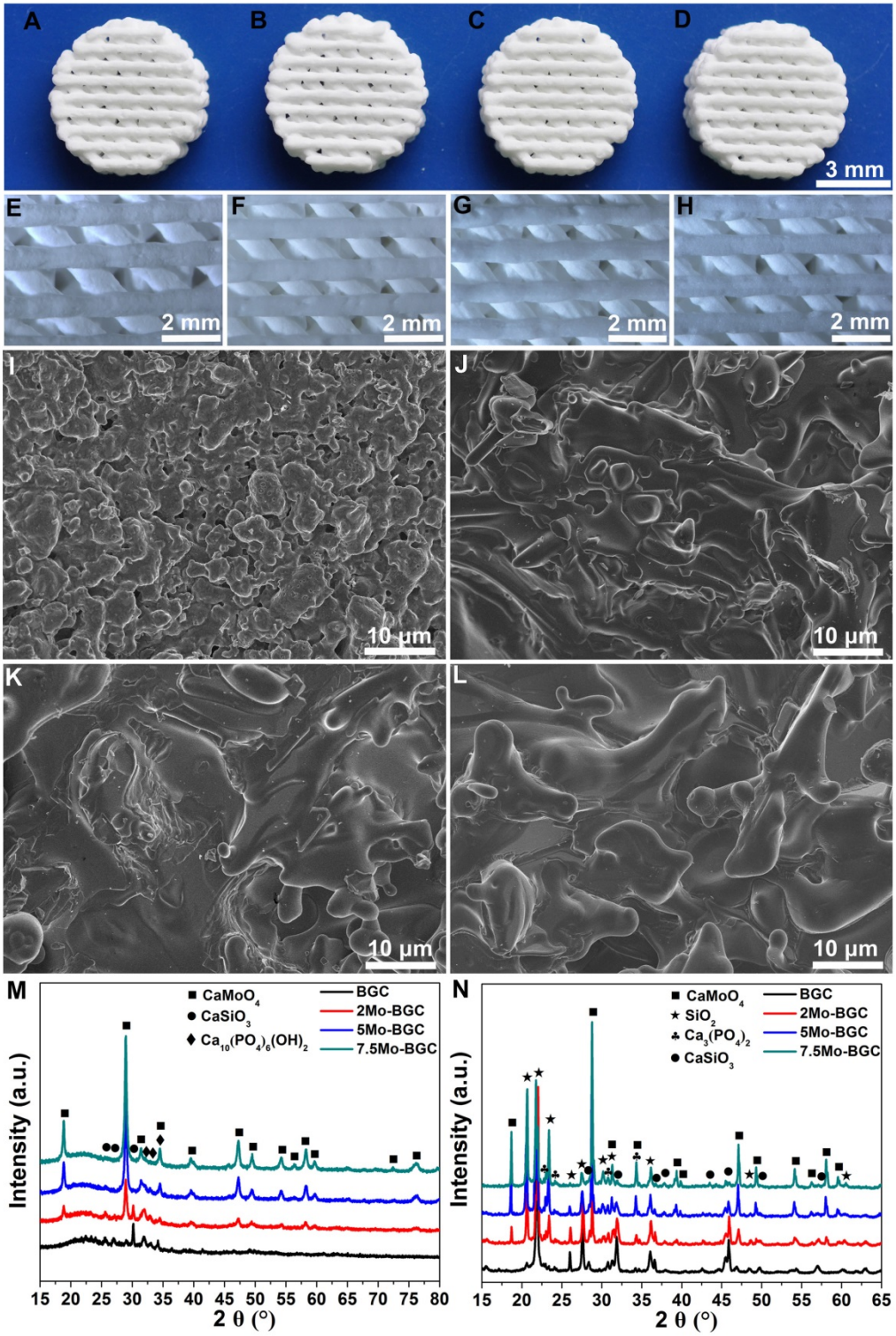

Figure 1. Photographs of 3D-printed BGC **(A)**, 2Mo-BGC **(B)**, 5Mo-BGC **(C)** and 7.5Mo-BGC **(D)** scaffolds. Optical microscopy images of BGC **(E)**, 2Mo-BGC **(F)**, 5Mo-BGC **(G)** and 7.5Mo-BGC **(H)** scaffolds. SEM images of BGC **(I)**, 2Mo-BGC **(J)**, 5Mo-BGC **(K)** and 7.5Mo-BGC **(L)** scaffolds. XRD patterns of BGC, (2, 5, 7.5)Mo-BGC powders calcined at 800 °C **(M)** and BGC, (2, 5, 7.5)Mo-BGC scaffolds sintered at 1350 °C **(N)**. The $CaMoO_4$ phase was able to regulate the surface morphology of the scaffolds and effectively improve the surface densification of Mo-BGC scaffolds.

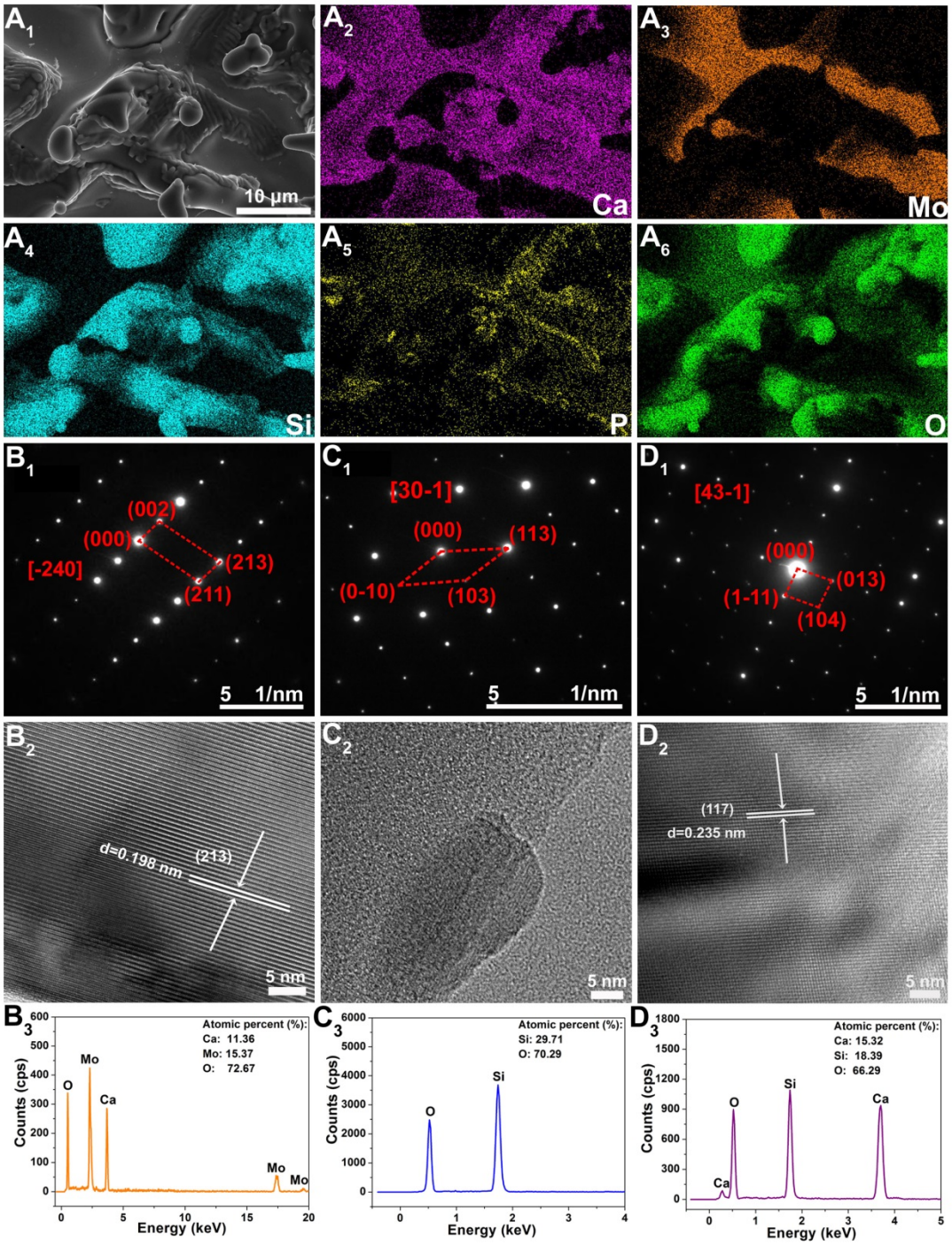

Figure 2. The element distribution images of 3D-printed 5Mo-BGC scaffold **(A_1-A_6)**. SAED patterns **(B_1, C_1, D_1)**, HRTEM images **(B_2, C_2, D_2)** and EDS analyses **(B_3, C_3, D_3)** of $CaMoO_4$ **(B_1-B_3)**, SiO_2 **(C_1-C_3)** and $CaSiO_3$ **(D_1-D_3)** crystals in 5Mo-BGC scaffold. $CaMoO_4$, SiO_2, and $CaSiO_3$ phases in the 5Mo-BGC scaffold were clearly identified in the form of monocrystal.

Compressive strength and degradation behavior of Mo-BGC scaffolds

The compressive strength results of BGC and (2, 5, 7.5)Mo-BGC scaffolds are shown in **Figure 3A-B**. The average compressive strengths of BGC, 2Mo-BGC, 5Mo-BGC and 7.5Mo-BGC were 11.77±0.65 MPa, 13.49±0.69 MPa, 17.66±1.20 MPa, 22.60±0.54 MPa, respectively. It could be seen that the compressive strength of BGC scaffolds was significantly improved through addition of Mo and the compressive strength of Mo-BGC scaffolds increased as the Mo content increased. The degradation behavior (**Figure 3C**) of BGC and (2, 5, 7.5)Mo-BGC scaffolds revealed that all the scaffolds could degrade in tris-HCl solution and the BGC scaffolds possessed the largest weight loss at the same time point. The weight losses of BGC, 2Mo-BGC, 5Mo-BGC, 7.5Mo-BGC scaffolds were respectively

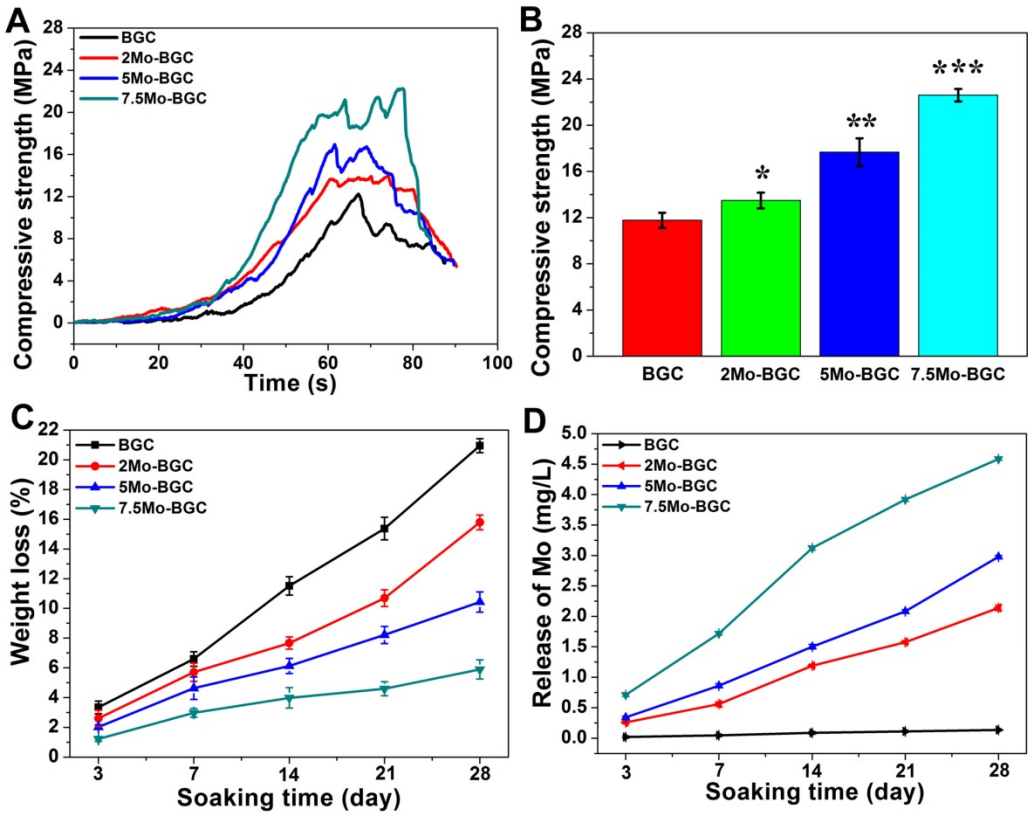

Figure 3. Compressive strength curves as a function of time **(A)** and compressive strength of BGC and (2, 5, 7.5)Mo-BGC scaffolds **(B)**. The degradation behavior of BGC and (2, 5, 7.5)Mo-BGC scaffolds immersed in tris-HCl solution **(C)**. The average release of Mo from scaffolds in tris-HCl solution at each time point **(D)**. The compressive strength of BGC scaffolds was remarkably enhanced by adding Mo. The Mo-BGC scaffolds degraded effectively and released Mo (MoO_4^{2-} ions) continuously.

calculated to be 20.95±0.47%, 15.79±0.50%, 10.43±0.68%, and 5.89±0.65% at day 28. The release rate of Mo (MoO_4^{2-} ions) from scaffolds immersed in tris-HCl solution is shown in **Figure 3D**. The release rates of Ca, Si and P from scaffolds are shown in **Figure S2**. BGC did not release Mo. From 2Mo-BGC to 7.5Mo-BGC, the release rate of Mo increased gradually, which was attributed to the increased Mo contents in the Mo-BGC scaffolds (**Table S1**). However, the release rates of Si and Ca exhibited the inverse trend as compared to Mo, which was consistent with the weight loss principle for BGC and Mo-BGC scaffolds. In addition, the release rates of P exhibited an inverse trend compared to Ca and Si. A possible reason is that Ca in the solution could inhibit the release of P through the common-ion effect because the release of P was accompanied by release of Ca from $Ca_3(PO_4)_2$.

In vitro proliferation and differentiation of RCs and HBMSCs cultivated with dilute solutions of 7.5Mo-BGC powder extract

Figure 4A and **Figure 4F** respectively show the proliferation levels of RCs (A) and HBMSCs (F) cultured with dilute solutions of BGC and 7.5Mo-BGC powder extracts (200 mg/mL). The RCs and HBMSCs presented different proliferation levels, which indicated that the ion concentration in dilute solution had a significant influence on their proliferation. Compared to BGC, nearly all the dilute solutions of 7.5Mo-BGC powder extract could enhance the proliferation of RCs at day 1, while only high concentrations of dilute solutions (1, 1/2, 1/4, 1/8 groups) of 7.5Mo-BGC powder extract could effectively promote proliferation of RCs at day 3 and 7. For HBMSCs, the proliferation performance did not show an obvious difference at day 1 when cultured with dilute solutions of BGC and 7.5Mo-BGC powder extracts, while nearly all the dilute solutions of 7.5Mo-BGC powder extract could promote the proliferation of HBMSCs at days 3 and 7 compared to BGC. The gene expressions related to chondrogenic differentiation of RCs (**Figure 4B-E**) and osteogenic differentiation of HBMSCs (**Figure 4G-J**) cultured with dilute solutions (1/2, 1/8 and 1/64 groups) of BGC and 7.5Mo-BGC powder extracts at day 7 are shown in **Figure 4**. It could be seen that all gene expressions related to chondrogenic and osteogenic differentiation in the dilute solutions were higher than those of the blank group. The expressions related to chondrogenic differentiation did not present obvious differences between the 1/2 group of dilute solutions of BGC and 7.5Mo-BGC powder extracts. The 1/8 dilute solution of 7.5Mo-BGC powder extract

significantly upregulated the gene expressions of SOX9, COL II, ACAN and N-cadh compared to BGC. The 1/64 dilute solution of 7.5Mo-BGC powder extract significantly upregulated the gene expressions of SOX9, COL II and ACAN compared to BGC. Therefore, it could be concluded that the low ion concentration of dilute solutions of 7.5Mo-BGC powder extract in the 1/8 and 1/64 groups better promoted chondrogenic differentiation compared to BGC. For the osteogenic differentiation of HBMSCs, the 1/2 dilute solution of 7.5Mo-BGC powder extract more significantly improved the expressions of OCN and BMP2 genes than BGC. The 1/8 dilute solution of 7.5Mo-BGC powder extract more significantly improved the gene expressions of COL I, BMP2 and RUNX2 than BGC, while the 1/64 dilute solution of 7.5Mo-BGC powder extract did not show obvious stimulation of the osteogenic differentiation of HBMSCs compared to BGC. In summary, the 1/8 dilute solution of 7.5Mo-BGC powder extract effectively enhanced chondrogenic differentiation of RCs and osteogenic differentiation of HBMSCs simultaneously as compared to BGC.

ALP and alizarin red stainings of HBMSCs cultivated with dilute solutions of 7.5Mo-BGC powder extract

Figure 5A-B shows ALP (A) and alizarin red (B) stained images of HBMSCs. 1/2, 1/8, and 1/64 dilute solutions of BGC and 7.5Mo-BGC powder extracts significantly stimulated ALP expression and enhanced the calcium nodule number in HBMSCs as compared to the blank group. The 1/8 group more effectively upregulated ALP expression and enhanced more calcium nodules compared to the other groups. In addition, the group exposed to 1/8 solution of 7.5Mo-BGC powder extract had more ALP expression and calcium nodules than the group exposed to BGC. The enhancement of ALP expression and calcium nodules indicated the early mineralization of osteogenic differentiation in HBMSCs. Therefore, it could be concluded that the 1/8 dilute solution of 7.5Mo-BGC powder extract could be more conducive to osteogenesis.

In vitro proliferation and attachment of RCs and HBMSCs on Mo-BGC scaffolds

Figure 6A-B shows the proliferation of RCs (A) and HBMSCs (B) cultured with BGC and Mo-BGC scaffolds. The results revealed that 7.5Mo-BGC scaffolds could significantly improve the proliferation of RCs and HBMSCs as compared to BGC. This effect was more obvious with cultivation. The 5Mo-BGC scaffolds significantly stimulated the proliferation of RCs at day 7 and stimulated the proliferation of HBMSCs at day 1, 3 and 7 as compared to BGC scaffolds. CLSM images of RCs at day 1, 7 and SEM images of RCs at day 7 seeding on BGC and 7.5Mo-BGC scaffolds are shown in **Figure 6C**. It could be seen that there were few RCs on the surface of BGC and 7.5Mo-BGC scaffolds at day 1 and there were more RCs at day 7, indicating that the RCs could proliferate well on the scaffolds over the culture time. The HBMSCs on the BGC and 7.5Mo-BGC scaffolds presented a similar performance to RCs (**Figure 6D**). Additionally, it could be seen that RCs on the 7.5Mo-BGC scaffold had better spread morphology than those on the BGC scaffold, and HBMSCs on the 7.5Mo-BGC scaffold had more abundant filopodia than those on the BGC scaffold, as observed by SEM and confocal laser scanning microscopy (CLSM).

Effect of MoO_4^{2-} ions on chondrogenic differentiation of RCs in a co-culture system

In order to investigate the effect of MoO_4^{2-} ions on the chondrogenic differentiation of co-cultured RCs as well as the related mechanism, different concentrations of MoO_4^{2-} ions were cultured with both RCs and HBMSCs in a co-culture system. The results showed that MoO_4^{2-} ions could be involved in motivating the anabolic responses of co-cultured RCs (**Figure 7**). The gene expression of hypoxia inducible factor-1α (HIF-1α) was remarkably upregulated by MoO_4^{2-} ions in the co-culture system, implying that the HIF-1α signaling pathway of co-cultured RCs was activated. The activated HIF-1α signaling pathway could stimulate the gene expression of chondrogenic differentiation molecular switch SOX9 that could further stimulate the gene expressions of COL II and ACAN, indicating that MoO_4^{2-} ions could promote the phenotype and chondrogenic differentiation of RCs.

Furthermore, the gene expression of hypoxia inducible factor-2α (HIF-2α) and its downstream catabolic factors including matrix metalloproteinases (MMP13), aggrecanase-2 (ADAMTS5) and key anticatabolic factor TIMP3 were also explored. The results showed that MoO_4^{2-} ions decreased the expression of HIF-2α, especially at high concentration. The expression of TIMP3 was highly upregulated by MoO_4^{2-} ions, while MMP13 and ADAMTS5 were effectively inhibited by MoO_4^{2-} ions. In summary, MoO_4^{2-} ions stimulated the anabolic responses of co-cultured RCs through initiating the HIF-1α signaling pathway, which was indicated by the upregulation of HIF-1α, SOX9, COL II and ACAN, and simultaneously inhibited the catabolic responses of co-cultured RCs, which was indicated by the downregulation of HIF-2α, MMP13, ADAMTS5 as well as upregulation of TIMP3.

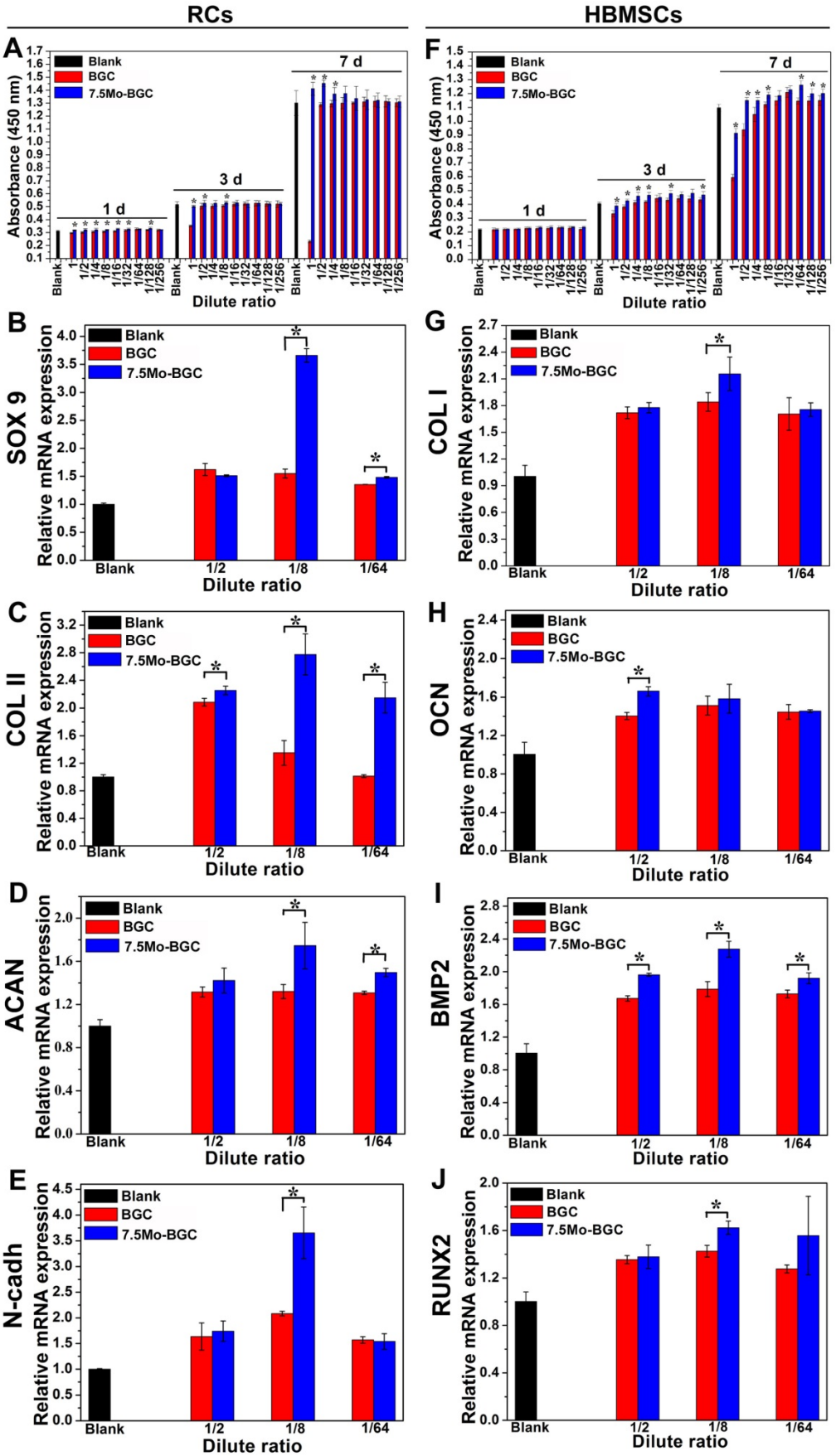

Figure 4. Proliferation of RCs **(A)** and HBMSCs **(F)** cultivated with dilute solutions of BGC and 7.5Mo-BGC powder extracts. The gene expressions of RCs **(B-E)** and HBMSCs **(G-J)** cultivated with 1/2, 1/8 and 1/64 dilute solutions of BGC and 7.5Mo-BGC powder extracts at day 7. The 1/8 dilute solution of 7.5Mo-BGC powder extract effectively enhanced chondrogenic differentiation of RCs and osteogenic differentiation of HBMSCs as compared to BGC.

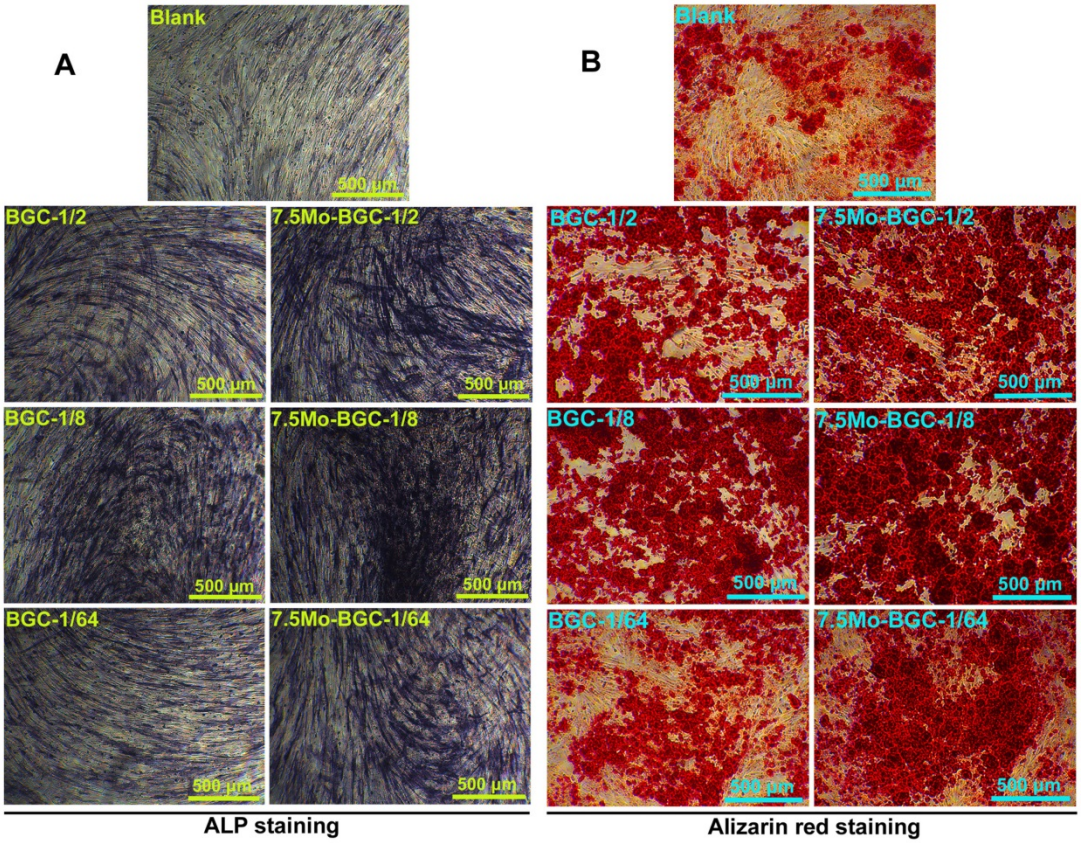

Figure 5. ALP staining **(A)** and alizarin red staining images **(B)** of HBMSCs cultured with 1/2, 1/8 and 1/64 dilute solutions of BGC and 7.5Mo-BGC powder extracts at day 7. The dilute solutions of 7.5Mo-BGC powder extract, especially the 1/8 group, improved the expression of ALP and simultaneously stimulated the formation of more calcium nodules as compared to BGC.

Effect of MoO_4^{2-} ions on chondrogenic differentiation of HBMSCs in a co-culture system

The related gene expressions of the HIF-1α signaling pathway in co-cultured HBMSCs were also analyzed. The gene expression of HIF-1α in groups treated with MoO_4^{2-} ions showed significant upregulation compared to the control group without MoO_4^{2-} ions, indicating that the HIF-1α signaling pathway of co-cultured HBMSCs was also activated by MoO_4^{2-} ions (**Figure 8**).

Simultaneously, the gene expressions of COL II and ACAN were remarkably enhanced by MoO_4^{2-} ions, indicating that the co-cultured HBMSCs could be induced to chondrogenic differentiation under stimulation by MoO_4^{2-} ions in the co-culture system. For the HIF-2α gene, there was no significant expression difference between all groups treated with MoO_4^{2-} ions and the control group. However, it was clear that MoO_4^{2-} ions not only remarkably upregulated the gene expression of TIMP3, but also significantly downregulated the gene expressions of MMP13 and ADAMTS5. Therefore, it can be concluded that MoO_4^{2-} ions promote anabolic responses of co-cultured HBMSCs in the co-culture system through activating the HIF-1α signaling pathway, and weaken catabolic responses through upregulating the expression of anticatabolic factor TIMP3, and simultaneously downregulating the expression of catabolic factors including MMP13 and ADAMTS5, finally stimulating the chondrogenic differentiation of co-cultured HBMSCs.

In vivo repair of osteochondral defects by 7.5Mo-BGC scaffolds

The *in vivo* repair efficacy of osteochondral defects by 7.5Mo-BGC scaffolds was evaluated in a rabbit osteochondral defect model. The representative overall appearance and micro-CT analysis results of knee joints collected at week 8 and 12 are shown in **Figure 9**. It could be seen that osteochondral defects of the blank group did not completely heal at week 8 and 12. The blank group had poor bone regeneration at week 8, indicated by the large residual void spaces with a few new tissues in the bottom. At week 12, even though some new tissues began to form and fill in the void space, there were remaining small void spaces according to the micro-CT analysis. For the BGC and 7.5Mo-BGC groups, the defects were ready for complete healing with some new tissues covering the tops of the scaffolds in the defects at week 8, and

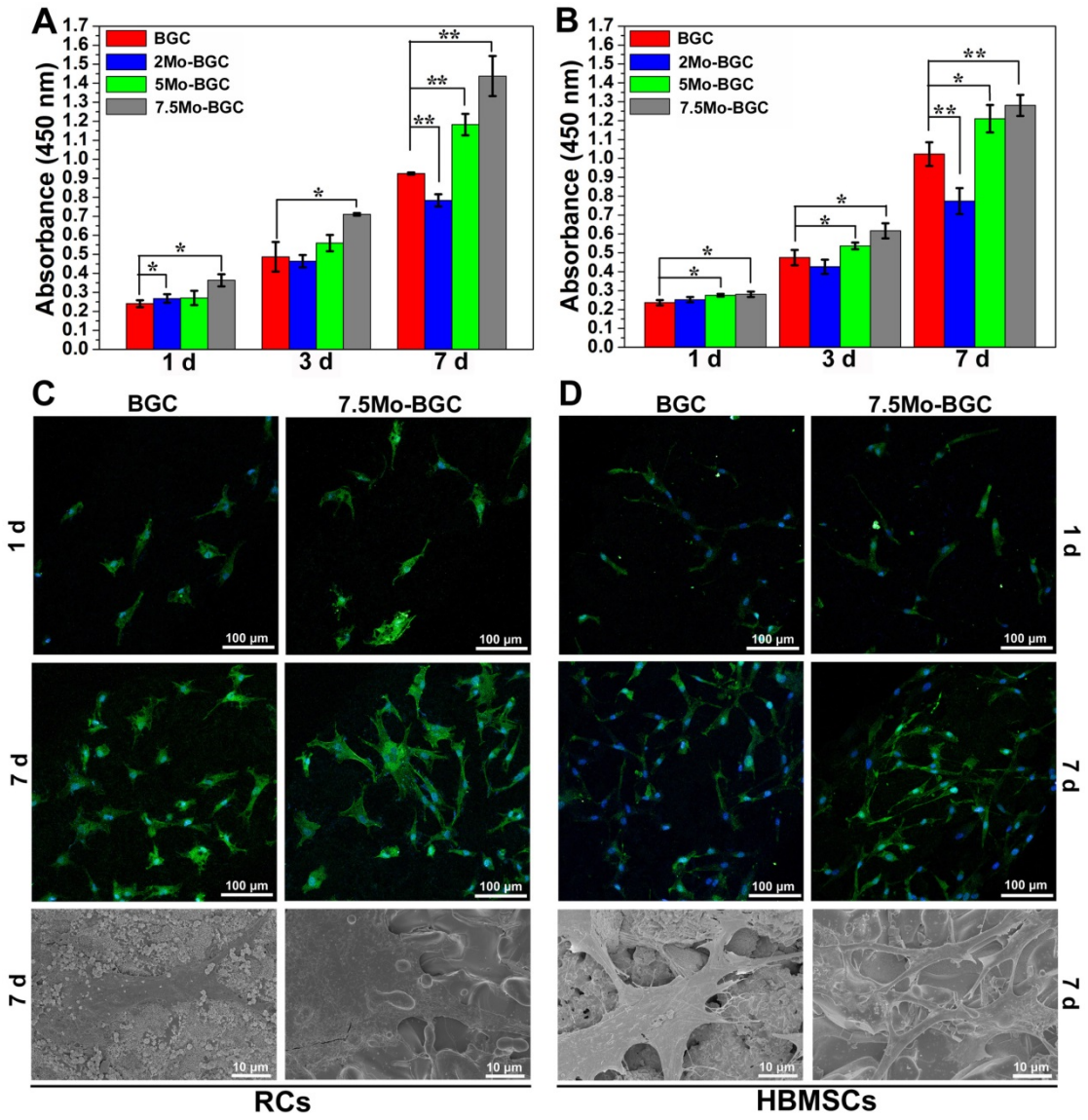

Figure 6. Proliferation of RCs **(A)** and HBMSCs **(B)** cultured with 3D-printed BGC and Mo-BGC scaffolds. **(C)** CLSM images at day 1, 7 and SEM images at day 7 of RCs cultured on BGC and 7.5Mo-BGC scaffolds. **(D)** CLSM images at day 1, 7 and SEM images at day 7 of HBMSCs cultured on BGC and 7.5Mo-BGC scaffolds. 7.5Mo-BGC scaffolds significantly promoted the proliferation of RCs and HBMSCs as compared to the BGC scaffolds.

the whole tops of the scaffolds in the defects had been covered by new tissue at week 12. It was hard to identify the repair capacity of BGC and 7.5Mo-BGC scaffolds only through the overall appearance of the collected knee joints. However, the 7.5Mo-BGC scaffolds had a better capacity for repairing defects than BGC scaffolds according to micro-CT analysis. The micro-CT analysis results showed that there were more new bone tissues (red color) surrounding and in the interior of the 7.5Mo-BGC scaffolds than BGC scaffolds, especially at week 12.

To further evaluate the efficacy of 7.5Mo-BGC scaffolds for repairing osteochondral defects, histological sections of defect positions in blank, BGC and 7.5Mo-BGC groups were stained by safranin O and alizarin red, and then analyzed. The safranin O staining results are shown in **Figure 10**. For the blank group at week 8, large residual void spaces were observed, indicating poor bone regeneration. For the BGC and 7.5Mo-BGC groups, some hyaline cartilage-like tissues, glycosaminoglycans (GAGs), which are an indispensable ingredient in the extracellular matrix of articular cartilage, were gradually forming on the tops of the scaffolds. At week 12, the tops and margins of the osteochondral defects in the blank group were covered by some GAGs, while there were still some residual void spaces inside the defects. For the BGC and 7.5Mo-BGC groups, numerous GAGs and some neo-bone tissues could be seen on the tops of the scaffolds. The 7.5Mo-BGC scaffolds exhibited more GAGs and neo-bone tissues than BGC scaffolds. In addition, some GAGs could be observed in the interior voids of the 7.5Mo-BGC scaffolds, indicating that 7.5Mo-BGC

scaffolds could be more conducive to generation of GAGs. The alizarin red staining results are shown in **Figure 11**. For the blank group, residual void spaces were very visible owing to the limited bone regeneration capacity at week 8 and some relatively small void spaces still remained at week 12. In contrast, 7.5Mo-BGC significantly promoted more new bone formation, which was characterized by more alizarin red than the blank and BGC groups. In addition, some new bone tissues filled the interior voids of the 7.5Mo-BGC scaffolds, indicating that 7.5Mo-BGC scaffolds possess a better ability to induce osteogenesis than BGC scaffolds.

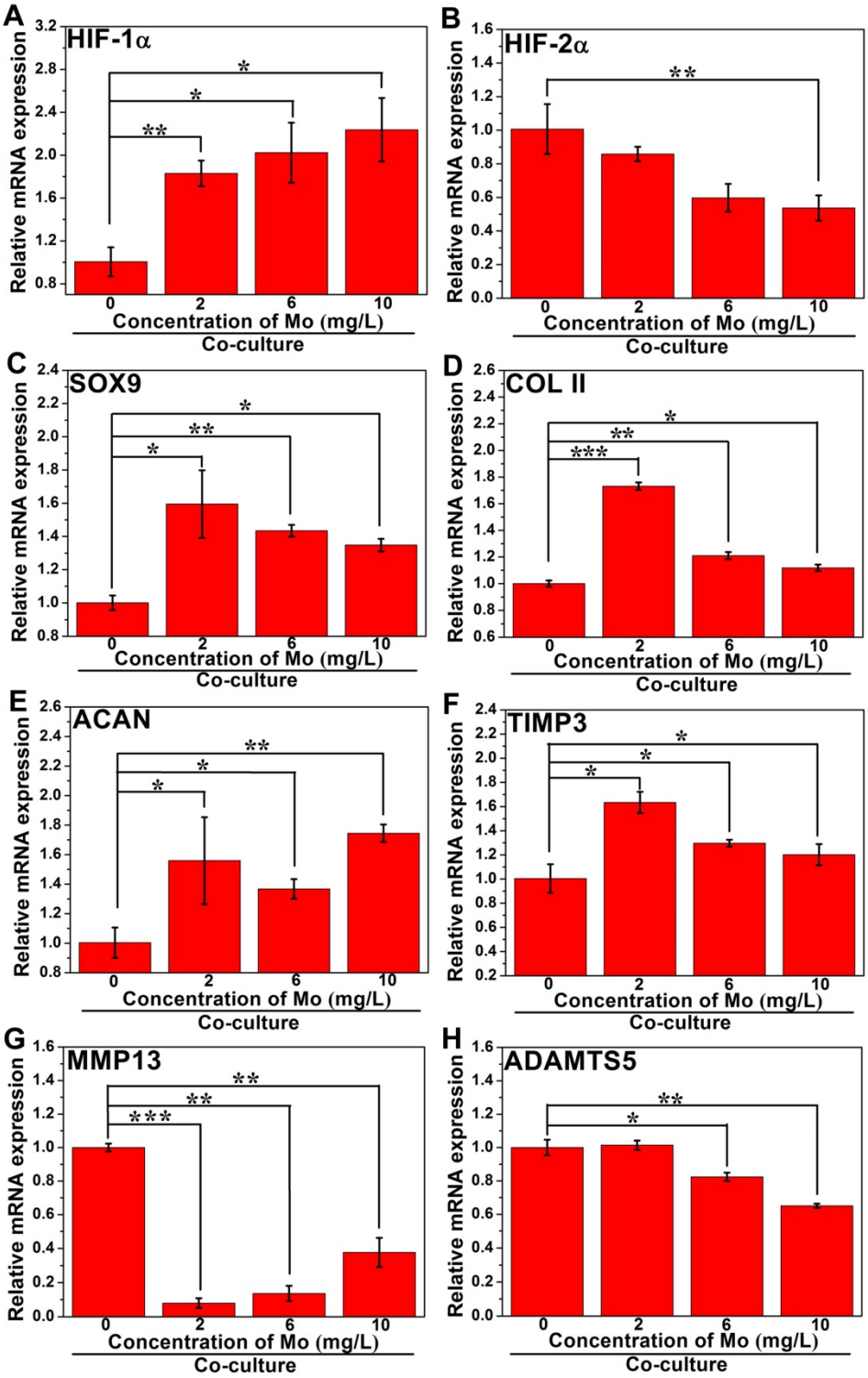

Figure 7. The effect of MoO_4^{2-} ions on the chondrogenic differentiation of co-cultured RCs. MoO_4^{2-} ions stimulated the anabolic responses of co-cultured RCs through initiating the HIF-1α signaling pathway, indicated by the upregulation of HIF-1α, SOX9, COL II, and ACAN genes expressions, and simultaneously inhibited the catabolic responses of co-cultured RCs, indicated by the downregulation of HIF-2α, MMP13, ADAMTS5 genes expressions as well as upregulation of TIMP3 gene expression.

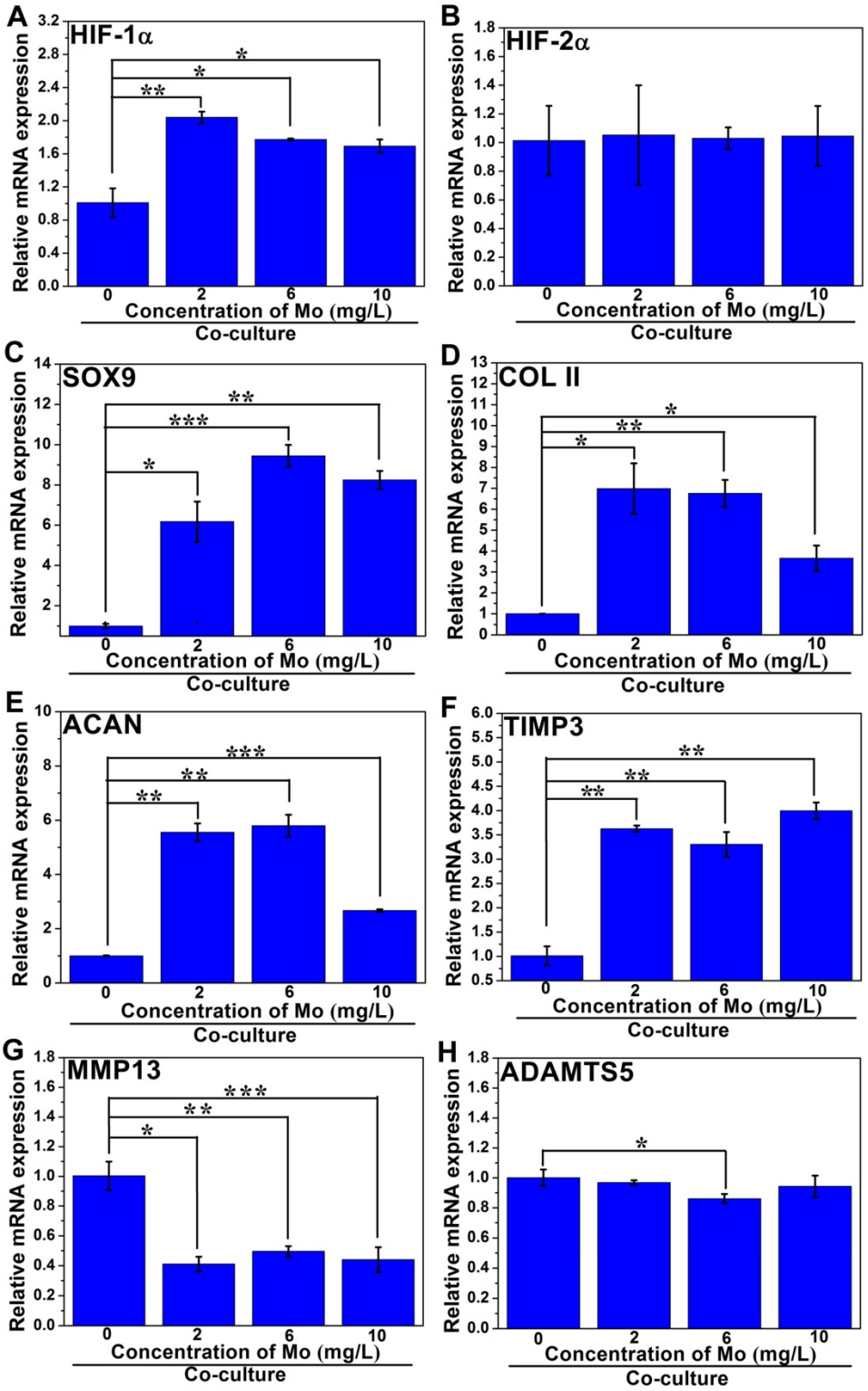

Figure 8. The effect of MoO_4^{2-} ions on the chondrogenic differentiation of HBMSCs in the co-culture system. MoO_4^{2-} ions promoted the anabolic responses of co-cultured HBMSCs through activating the HIF-1α signaling pathway, indicated by the upregulation of HIF-1α, SOX9, COL II, and ACAN genes expressions, and weakened catabolic responses through downregulating the expressions of MMP13 and ADAMTS5 genes, and simultaneously upregulating the expression of TIMP3 gene.

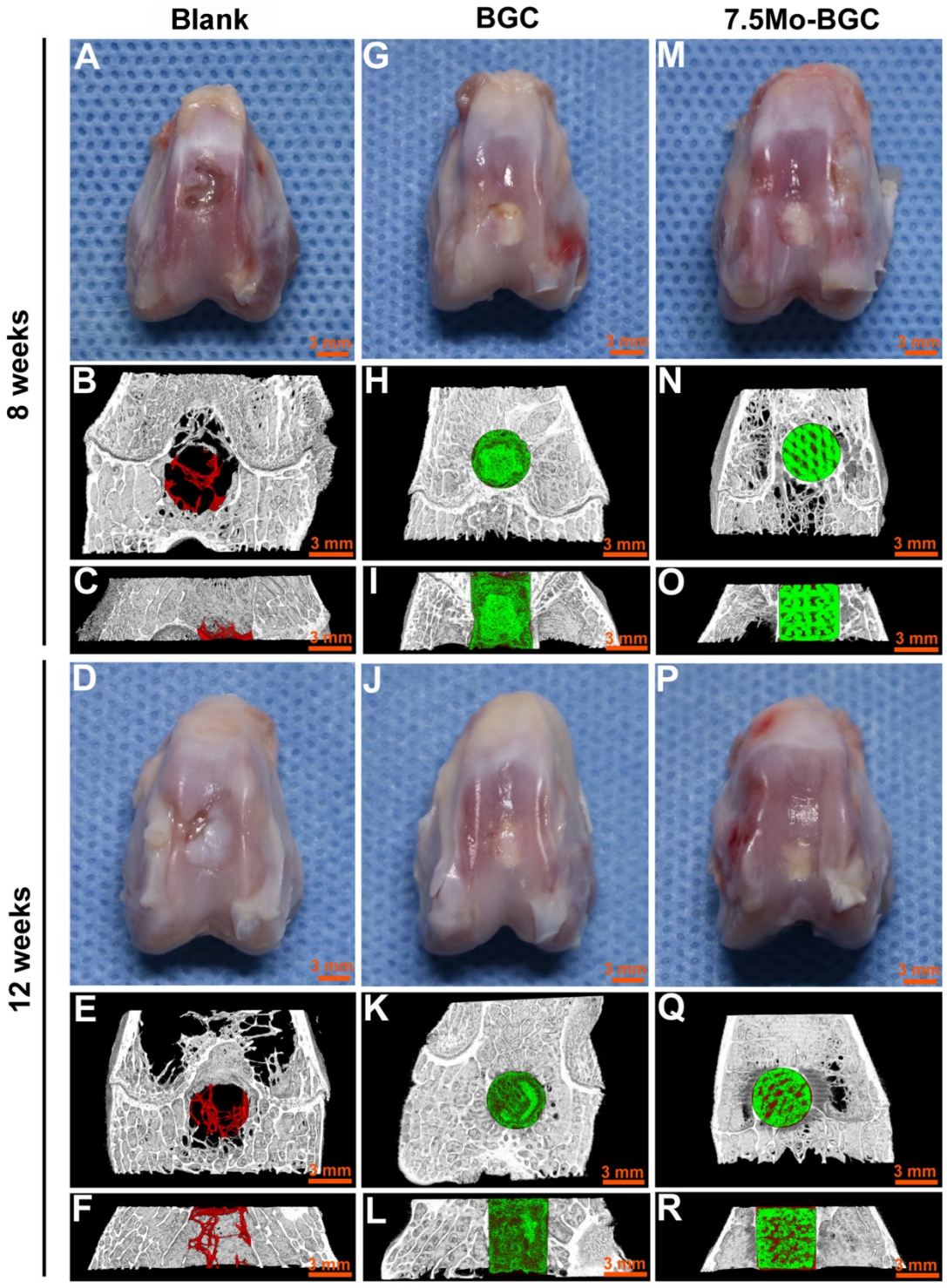

Figure 9. Digital photographs and micro-CT imaging analyses of defects in blank, BGC and 7.5Mo-BGC groups at weeks 8 and 12. Digital photographs showed the overall appearance of defects of blank **(A)**, BGC **(G)**, and 7.5Mo-BGC **(M)** groups at week 8 and blank **(D)**, BGC **(J)**, and 7.5Mo-BGC **(P)** groups at week 12. The transverse view of 3D reconstruction images of blank **(B)**, BGC **(H)**, and 7.5Mo-BGC **(N)** groups at week 8 and blank **(E)**, BGC **(K)**, and 7.5Mo-BGC **(Q)** groups at week 12. The vertical view of 3D reconstruction images of blank **(C)**, BGC **(I)**, and 7.5Mo-BGC **(O)** groups at week 8 and blank **(F)**, BGC **(L)**, and 7.5Mo-BGC **(R)** groups at week 12. In the 3D reconstruction images, the off-white, red and green colors stand for primary bone, new bone, and scaffold, respectively. Digital photographs and micro-CT analyses of osteochondral defects demonstrated that 7.5Mo-BGC effectively enhanced the regeneration of both cartilage and subchondral bone as compared to blank and BGC groups at weeks 8 and 12.

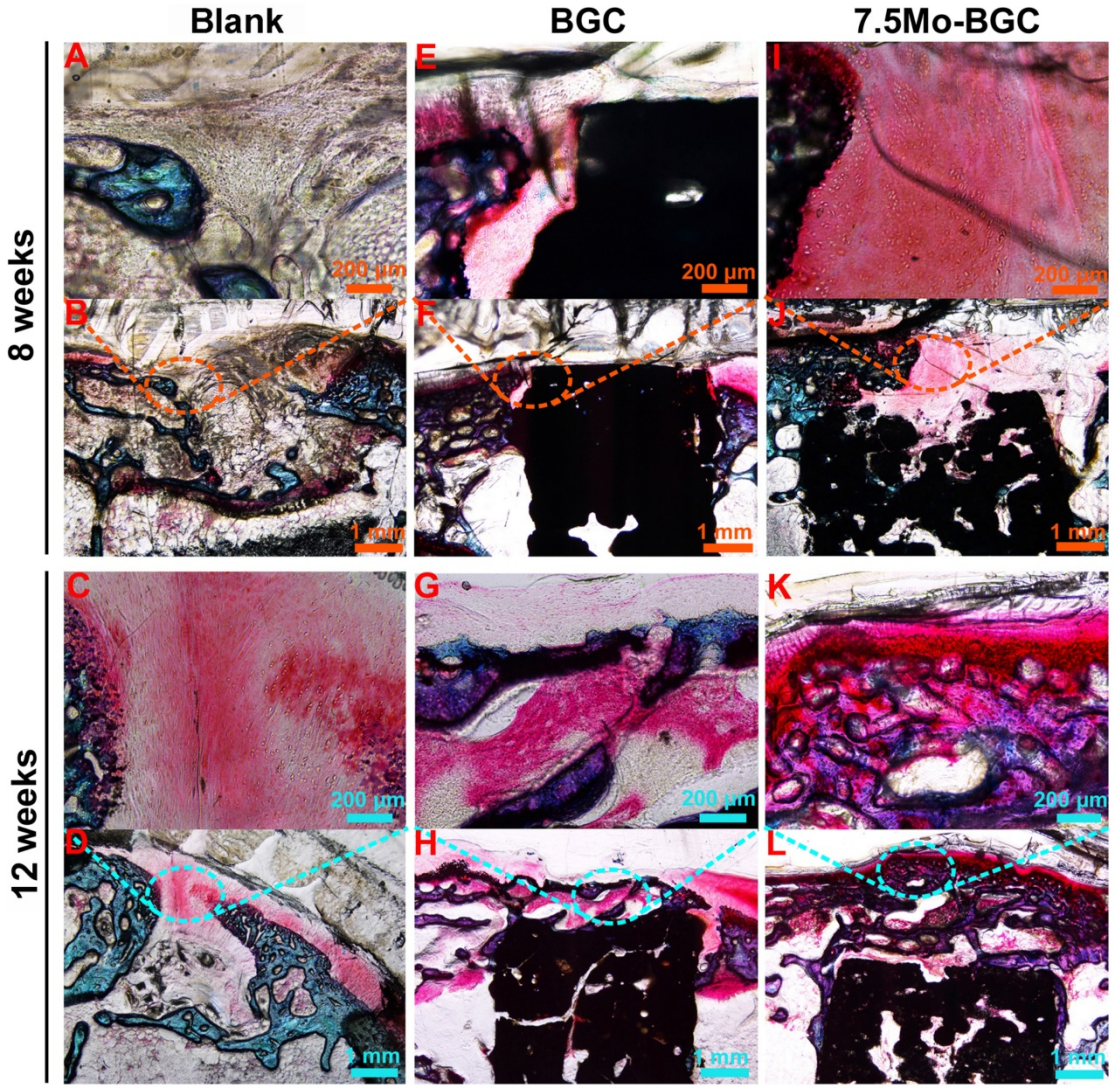

Figure 10. *In vivo* articular cartilage regeneration evaluation by safranin O staining. Safranin O-stained images of blank **(A-B)**, BGC **(E-F)**, and 7.5Mo-BGC **(I-J)** groups at week 8 and blank **(C-D)**, BGC **(G-H)**, and 7.5Mo-BGC **(K-L)** groups at week 12. The safranin O staining results showed that the 7.5Mo-BGC group possessed more hyaline cartilage-like tissues than the blank and BGC groups.

Discussion

Molybdenum (Mo) is an essential trace element for plants, animals and microorganisms and it constitutes several Mo-enzymes that play important roles in physiology. Even though a few investigations have focused on preparing bioactive glass ceramics containing Mo, the effects of Mo on RCs and HBMSCs as well as the application of Mo to bone tissue engineering have not been reported so far. Therefore, Mo-BGC scaffolds were successfully fabricated through combining a sol-gel method with 3D printing technique. The effects of Mo in the bioactive glass on the maturation, proliferation and differentiation of RCs and HBMSCs were firstly systematically investigated. Finally, the 7.5Mo-BGC scaffolds were applied to osteochondral defects to evaluate their prospect in bone tissue engineering.

When introducing Mo into the bioactive glass, Mo reacted with Ca and O elements to form $CaMoO_4$ phase during the calcining process at 800 °C, as evidenced by XRD characterization. After sintering at 1350 °C, the Mo-BGC scaffolds were composed of $CaMoO_4$, SiO_2, and $CaSiO_3$ and $Ca_3(PO_4)_2$ phases. It was interesting that the incorporation of Mo into the bioactive glass scaffolds significantly enhanced the compressive strength of the scaffolds and the compressive strength increased as the Mo content increased. In addition, the weight loss of the scaffolds decreased as the Mo content increased. The related reasons are described as follows: When the original 3D-printed scaffolds were sintered at 1350 °C, the $CaMoO_4$ phase melted because of its low melting point (965 °C). The melted $CaMoO_4$ phase plays an important role in connecting other phases such as SiO_2, $CaSiO_3$ and $Ca_3(PO_4)_2$, as shown in the EDS images and boosts the surface densification of the

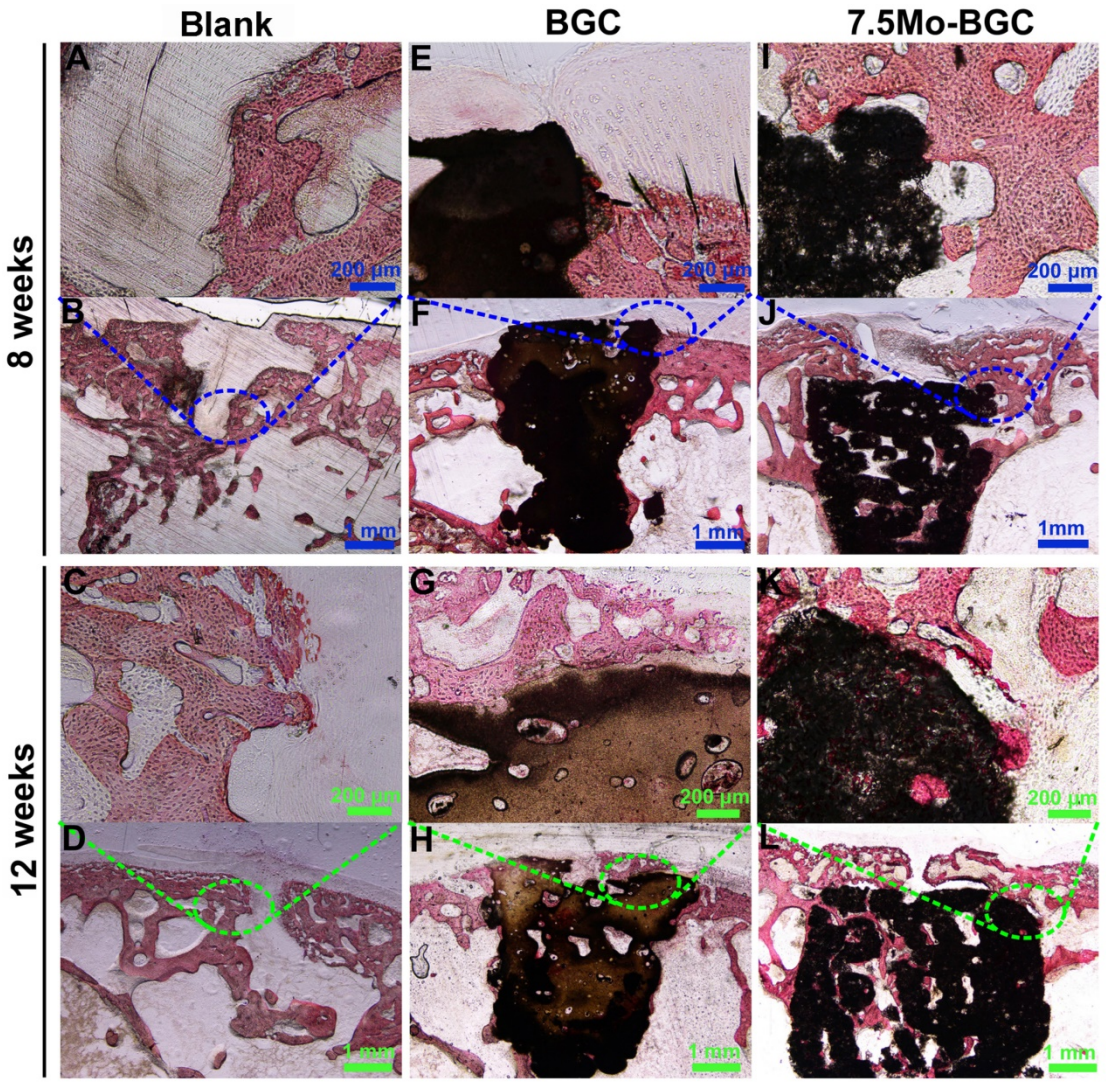

Figure 11. *In vivo* subchondral bone regeneration evaluation by alizarin red staining. Alizarin red-stained images of blank **(A-B)**, BGC **(E-F)**, and 7.5Mo-BGC **(I-J)** groups at week 8 and blank **(C-D)**, BGC **(G-H)**, and 7.5Mo-BGC **(K-L)** groups at week 12. The alizarin red staining results showed that 7.5Mo-BGC better promoted the formation of subchondral bone than the blank and BGC groups.

scaffolds. According to the SEM images in **Figure 1I-L**, the surface of the scaffold became more compact with the increase of Mo content and some micropores in the BGC scaffold disappeared. The improved densification of the scaffolds could be beneficial for enhancement of their compressive strength. Therefore, the compressive strength of the scaffolds increased as the Mo content increased. During evaluation of the degradation behavior of BGC and Mo-BGC, it was found that the weight loss of the scaffold decreased as the Mo content increased. A possible reason is that the improved surface densification of Mo-BGC scaffolds decreases the micropores and makes the surface contact area between the scaffolds and tris-HCl solution decrease in comparison with BGC scaffold.

One important result from this study is that the prepared 7.5Mo-BGC powder extract significantly promoted the proliferation and differentiation of RCs and HBMSCs *in vitro*. The proliferation results of RCs cultured with dilute solutions of BGC and 7.5Mo-BGC powder extracts (200 mg/mL) showed that high concentration (1, 1/2, 1/4, 1/8 groups) of 7.5Mo-BGC powder extract promoted proliferation of RCs more than BGC with cultivation. The expression levels of typical markers (COL II, ACAN, SOX9 and N-cadh) for chondrogenic differentiation in the cells treated with 1/8 and 1/64 dilute solutions of 7.5Mo-BGC powder extract were also significantly improved as compared to those of cells treated with BGC. The *in vitro* proliferation results of HBMSCs showed that 1/2, 1/8 and 1/64 dilute solutions of 7.5Mo-BGC powder extract more effectively stimulated the proliferation of HBMSCs at day 3 and day 7 than BGC. The expression levels of typical markers (COL I, BMP2, OPN, and RUNX2) for osteogenic

differentiation in the group treated with 1/8 dilute solution of 7.5Mo-BGC powder extract were significantly improved compared to those of the BGC group, indicating that the 1/8 solution could effectively promote osteogenic differentiation. In addition, there existed obvious gene expression level differences of SOX9, N-cadh, BMP2 between different groups treated with dilute solutions of 7.5Mo-BGC powder extract. However, most of the gene expressions did not have apparent differences between different groups of dilute solutions of BGC powder extract. Therefore, it could be inferred that MoO_4^{2-} ions played a critical role in regulating gene expressions related to chondrogenic and osteogenic differentiation. And, different concentrations of MoO_4^{2-} ions could discriminatively regulate gene expression. Gene expression largely depends on ionic concentration, which has been reported in the literature. For example, Deng *et al.* investigated the effect of Mn^{2+} on chondrogenesis. The results showed that the N-cadh gene expression level increased with the increase of Mn^{2+} concentration when the Mn^{2+} concentration was in the range of 0-0.5 μg/mL, while the N-cadh gene expression level decreased with an increase of Mn^{2+} concentration when the Mn^{2+} concentration was in the range of 0.5-2.0 μg/mL [39]. Mao *et al.* investigated the synergistic effect of bioactive Sr and Si ions on osteogenesis, osteoclastogenesis and angiogenesis. The results showed that the gene expression level of OPN/RANKL stimulated by 3.07 mg/L Sr ions was higher than that of the blank group, while the gene expression level of OPN/RANKL stimulated by 6.15 mg/L Sr ions decreased compared to treatment with 3.07 mg/L Sr ions [40]. Therefore, it could be concluded that the concentration of bioactive ions plays a vital role in regulating gene expression. When the ion species is the same, each gene has the optimal ionic concentration range to stimulate its expression. When the HBMSCs were cultured with dilute solutions of 7.5Mo-BGC powder extract, ALP gene expression and calcium deposit formation in HBMSCs were significantly enhanced as compared to those cells treated with BGC. The ALP gene expression upregulation marked early mineralization of osteogenic differentiation in HBMSCs. Additionally, the 7.5Mo-BGC scaffolds also significantly improved the proliferation and attachment of RCs and HBMSCs *in vitro* as compared to BGC.

Another interesting result was that 3D-printed 7.5Mo-BGC scaffolds not only promoted the preservation of hyaline cartilage-like tissues, but also stimulated the reconstruction of subchondral bone *in vivo*. In the past, different types of scaffolds have been developed to repair osteochondral defects, such as biphasic, triphasic, and multilayered gradient scaffolds, but they could not biologically mimic the natural structure and functional properties of cartilage and subchondral bone. Moreover, different kinds of signaling molecules have been incorporated into scaffolds to further enhance their efficacy for repairing osteochondral defects [41, 42]. However, some adverse side effects would be caused by these signaling molecules [43, 44]. Therefore, our prepared single scaffold shows some distinct advantages through repairing cartilage/bone defects simultaneously.

In order to investigate the underlying mechanism of MoO_4^{2-} ions affecting chondrogenic differentiation, a co-culture system of RCs and HBMSCs was established based on the following considerations. A co-culture system can better mimic the native cartilage microenvironment *in vivo*. Additionally, a co-culture of both chondrocytes and HBMSCs has been extensively reported to effectively prevent the dedifferentiation of chondrocytes and could reduce the number of chondrocytes needed [45-47]. Therefore, the adoption of an *in vitro* RCs and hBMSCs co-culture model helped to more objectively investigate the effect of MoO_4^{2-} ions on chondrogenesis. The potential mechanism of 7.5Mo-BGC promoting RCs maturation and cartilage regeneration may be closely related to MoO_4^{2-} ions activating anabolic responses (HIF-1α signaling pathway) and suppressing catabolic responses. It was reported that HIF-1α, as an important regulator of cartilage homeostasis, could induce chondrogenesis by regulating the expression of chondrogenic differentiation molecular switch SOX9 in hypoxic pre-chondrogenic cells and protect articular cartilage through promoting the chondrocyte phenotype, maintaining chondrocyte viability, and supporting metabolic adaptation to a hypoxic environment [48-50]. The results showed that HIF-1α signaling pathway was activated by MoO_4^{2-} ions in RCs and the upregulated HIF-1α further promoted the expression of SOX9, which subsequently enhanced the expression of COL II and ACAN, indicating that MoO_4^{2-} ions could promote the phenotype and chondrogenic differentiation of chondrocytes.

HIF-2α is a catabolic transcription factor in the osteoarthritic process and it directly induces the expression of catabolic factors in chondrocytes such as matrix metalloproteinases and aggrecanase, and finally causes cartilage destruction and accelerates osteoarthritis progression [48, 51, 52]. Additionally, the MMP13 and ADAMTS5 are able to degrade COL II, lead to articular cartilage destruction and initiate osteoarthritis [53-56]. Meanwhile, TIMP3, a key anticatabolic factor and one of the endogenous

inhibitors of MMP13 and ADAMTS5 [57-59], was also studied. The results showed that MoO_4^{2-} ions inhibited catabolic responses of co-cultured RCs indicative of downregulation of HIF-2α, MMP13, ADAMTS5 as well as upregulation of TIMP3.

It was noteworthy that the gene expression levels of COL II and MMP13 in RCs and HBMSCs stimulated by different concentrations of MoO_4^{2-} ions were obviously different, which further suggested that ionic concentration plays a vital role in regulating gene expression, as previously discussed. When the concentration of Mo in MoO_4^{2-} increased from 0 to 10 mg/L, the COL II gene expression level decreased gradually. It could be concluded that the low concentration of MoO_4^{2-} ions was more beneficial for COL II gene expression. Even so, the COL II gene expression level stimulated by 10 mg/L of Mo was still higher than that of the control group (0 mg/L), which indicated that high concentration of MoO_4^{2-} ions could also play a role in promoting anabolism. MMP13 is a catabolic factor, which has the opposite effect of anabolic factors such as COL II, and can degrade cartilage matrix. Here, the MMP13 gene expression level increased as the Mo concentration increased. When the Mo concentration was 2 mg/L, the gene expression level of MMP13 was lowest, which indicated that the low concentration of MoO_4^{2-} ions could protect cartilage matrix from the degradation of MMP13 to a large extent and played an important role in inhibiting catabolism. Conversely, at high concentration of Mo (e.g., 10 mg/L), the gene expression level of MMP13 was still lower than that of the control group, which indicated that a high concentration of MoO_4^{2-} ions could also play a part in inhibiting catabolism. This result was consistent with the gene COL II expression. Similarly, the related gene expressions of anabolic responses (HIF-1α signaling pathway) and catabolic responses in HBMSCs co-cultured with RCs and MoO_4^{2-} ions were also analyzed. The results showed that MoO_4^{2-} ions promoted anabolic responses of co-cultured HBMSCs through activating the HIF-1α signaling pathway and weakened catabolic responses through upregulating the expression of anticatabolic factor TIMP3, and simultaneously downregulating the expression of catabolic factors including MMP13 and ADAMTS5, and finally stimulated the chondrogenic differentiation of co-cultured HBMSCs.

Conclusion

In this study, Mo-BGC scaffolds were successfully prepared through combining a sol-gel method with 3D printing technique. The incorporation of Mo into BGC not only effectively enhanced the surface density and compressive strength of BGC scaffolds, but also significantly stimulated the proliferation and differentiation of both RCs and HBMSCs *in vitro*. Moreover, 7.5Mo-BGC scaffolds showed bi-lineage bioactivities for regeneration of articular cartilage and subchondral bone tissues *in vivo*. The related mechanisms are that the MoO_4^{2-} ions not only triggered anabolic responses and stimulated chondrogenesis of co-cultured RCs and HBMSCs through activating the HIF-1α signaling pathway, but also restrained catabolic responses through upregulating the expression of anticatabolic factor TIMP3 and downregulating the expressions of catabolic factors MMP13 and ADAMTS5. These results suggest that Mo-BGC scaffolds with activated anabolic responses can biologically satisfy the requirement for regenerating articular cartilage and subchondral bone tissues simultaneously, providing a more extensive selection for cartilage/bone regeneration.

Supplementary Material

Supplementary figures and tables.
http://www.thno.org/v08p4372s1.pdf

Acknowledgements

This work was supported by the National Key Research and Development Program of China (2018YFB1105501), the Natural Science Foundation of China (5171101275, 81771989, 81601612), Key Research Program of Frontier Sciences CAS (QYZDB-SSW-SYS027) and Science and Technology Commission of Shanghai Municipality (17441903700, 16DZ2260603, 17540712300) and Key Research Program of Science & Technology Support Program of Jiangsu Province (BE2016763).

Competing Interests

The authors have declared that no competing interest exists.

References

1. Mow VC, Ratcliffe A, Poole AR. Cartilage and diarthrodial joints as paradigms for hierarchical materials and structures. Biomaterials. 1992; 13: 67.
2. Du YY, Liu HM, Yang Q, et al. Selective laser sintering scaffold with hierarchical architecture and gradient composition for osteochondral repair in rabbits. Biomaterials. 2017; 137: 37-48.
3. Seo SJ, Mahapatra C, Singh RK, Knowles JC, Kim HW. Strategies for osteochondral repair: focus on scaffolds. J Tissue Eng M. 2014; 5: 1-14.
4. Shi J, Liang JI, Guo BY, et al. Adipose-derived stem cells cocultured with chondrocytes promote the proliferation of chondrocytes. Stem Cells Int. 2017; 1709582.
5. Öztürk E, Arlov Ø, Aksel S, et al. Sulfated hydrogel matrices direct mitogenicity and maintenance of chondrocyte phenotype through activation of FGF signaling. Adv Funct Mater. 2016; 26: 3649-3662.
6. Chen ZL, Yan CG, Yan SN, et al. Non-invasive monitoring of in vivo hydrogel degradation and cartilage regeneration by multiparametric MR imaging. Theranostics. 2018; 8(4): 1146-1158.
7. Liao JF, Shi K, Ding QX, et al. Recent developments in scaffold-guided cartilage tissue regeneration. J Biomed Nanotechnol. 2014; 10(10): 3085-3104.

8. Meng FG, Li ZW, Zhang ZQ, et al. MicroRNA-193b-3p regulates chondrogenesis and chondrocyte metabolism by targeting HDAC3. Theranostics. 2018; 8(10): 2862-2883.
9. Makitsubo M, Adachi N, Nakasa T, et al. Differences in joint morphology between the knee and ankle affect the repair of osteochondral defects in a rabbit model. J Ortho Surg Res. 2016; 11:110.
10. Li G, Fu N, Xie J, et al. Poly(3-hydroxybutyrate-co-4-hydroxybutyrate) based electrospun 3D scaffolds for delivery of autogeneic chondrocytes and adipose-derived stem cells: evaluation of cartilage defects in rabbit. J Biomed Nanotechnol. 2015; 11(1): 105-116.
11. Falah M, Nierenberg G, Soudry M, Hayden M, Volpin G. Treatment of articular cartilage lesions of the knee. Int Orthop. 2010; 34 (5): 621.
12. Vonk LA, Van-Dooremalen SFG, Liv N, et al. Mesenchymal stromal/stem cell-derived extracellular vesicles promote human cartilage regeneration in vitro. Theranostics. 2018; 8(4): 906-920.
13. Breinan HA, Martin SD, Hsu HP, Spector M. Healing of canine articular cartilage defects treated with microfracture, a type-II collagen matrix, or cultured autologous chondrocytes. J Orthop Res. 2000; 18: 781-789.
14. Steadman JR, Rodkey WG, Rodrigo JJ. Microfracture: surgical technique and rehabilitation to treat chondral defects. Clin Orthop Relat Res. 2001; 391(Suppl): S362-S369.
15. Brittberg M, Lindahl A, Nilsson A. Treatment of deep cartilage defects in the knee with autologous chondrocyte transplantation. N Engl J Med. 1994; 331: 889-895.
16. Dahlin RL, Kinard LA, Lam J, et al. Articular chondrocytes and mesenchymal stem cells seeded on biodegradable scaffolds for the repair of cartilage in a rat osteochondral defect model. Biomaterials. 2014; 35: 7460-7469.
17. Albrecht C, Tichy B, Nurnberger S, et al. Gene expression and cell differentiation in matrix-associated chondrocyte transplantation grafts: a comparative study. Osteoarthritis Cartilage. 2009; 19 (10): 1219-1227.
18. Dang WT, Li T, Li B, et al. A bifunctional scaffold with $CuFeSe_2$ nanocrystals for tumor therapy and bone reconstruction. Biomaterials. 2018; 160: 92-106.
19. Park H, Lim DJ, Lee SH, Park H. Nanofibrous mineralized electrospun scaffold as a substrate for bone tissue regeneration. J Biomed Nanotechnol. 2016; 12(11): 2076-2082.
20. Chen Y, Liu XY, Liu R, et al. Zero-order controlled release of BMP2-derived peptide P24 from the chitosan scaffold by chemical grafting modification technique for promotion of osteogenesis in vitro and enhancement of bone repair in vivo. Theranostics. 2017; 7 (5): 1072-1087.
21. Wang H, Zhang XR, Wang HC, et al. Enhancing the osteogenic differentiation and rapid osseointegration of 3D printed Ti6Al4V implants via nano-topographic modification. J Biomed Nanotechnol. 2018; 14 (4): 707-715.
22. Choi YJ, Yi HG, Kim SW, Cho DW. 3D cell printed tissue analogues: A new platform for theranostics. Theranostics. 2017; 7 (12): 3118-3137.
23. Yu YJ, Ren SS, Yao YF, et al. Electrospun fibrous scaffolds with iron-doped hydroxyapatite exhibit osteogenic potential with static magnetic field exposure. J Biomed Nanotechnol. 2017; 13(7): 835-847.
24. Sobral JM, Caridade SG, Sousa RA, Mano JF, Reis RL. Three dimensional plotted scaffolds with controlled pore size gradients: effect of scaffold geometry on mechanical performance and cell seeding efficiency. Acta Biomater. 2011; 7 (3): 1009-1018.
25. Singh M, Dormer N, Salash JR, et al. Three-dimensional macroscopic scaffolds with a gradient in stiffness for functional regeneration of interfacial tissues. J Biomed Mater Res A. 2010; 94A (3): 870-876.
26. Mohan N, Dormer NH, Caldwell KL, et al. Continuous gradients of material composition and growth factors for effective regeneration of the osteochondral interface. Tissue Eng Part A. 2011; 17 (21-22): 2845-2855.
27. Deng CJ, Zhu HY, Li JY, et al. Bioactive scaffolds for regeneration of cartilage and subchondral bone interface. Theranostics. 2018; 8 (7): 1940-1955.
28. Luca AD, Blitterswijk CV, Moroni L. The osteochondral interface as a gradient tissue: from development to the fabrication of gradient scaffolds for regenerative medicine. Birth Defects Reseach (Part C). 2015; 37 (105): 34-52.
29. Asadi F, Mohseni M, Noshahr KD, et al. Effect of molybdenum nanoparticles on blood cells, liver enzymes, and sexual hormones in male rats. Biol Trace Elem Res. 2017; 175 (1): 50-56.
30. Kikuchi K, Hamano S, Mochizuki H. Molybdenum cofactor deficiencymimics cerebral palsy: differentiating factors for diagnosis. Pediatr Neurol. 2012; 47 (2): 147-149.
31. Burguera JL, Burguera M. Molybdenum in human whole blood of adult residents of the Merida state (Venezuela). J Trace Elem Med Biol. 2007; 21 (3): 178-183.
32. Mendel RR. Molybdenum: Biological activity and metabolism. Dalton Trans. 2005; 21: 3404-3409.
33. Mendel RR. Cell biology of molybdenum. Biofactors. 2009; 35 (5): 429-434.
34. Xin Z, Xiang N, Chen J, Wei B. In vitro biocompatibility of Co-Cr alloy fabricated by selective laser melting or traditional casting techniques. Mater Lett. 2012; 88: 101-103.
35. Kyomoto M, Iwasaki Y, Moro T, et al. High lubricious surface of cobalt-chromium-molybdenum alloy prepared by grafting poly (2-methacryloyloxyethyl phosphorylcholine). Biomaterials. 2007; 28 (20): 3121-3130.
36. Qin LG, Zeng QF, Wang WX, Zhang YL, Dong GN. Response of MC3T3-E1 osteoblast cells to the microenvironment produced on Co-Cr-Mo alloy using laser surface texturing. J Mater Sci. 2014; 49: 2662-2671.
37. Kanaji A, Orhue V, Caicedo MS, et al. Cytotoxic effects of cobalt and nickel ions on osteocytes in vitro. J Ortho Surg Res. 2014; 9: 91.
38. Mainil-Varlet P, Aigner T, Brittberg M, et al. Histological assessment of cartilage repair-a report by the histology endpoint committee of the international cartilage repair society (ICRS). J Bone Jt Surg Am Vol. 2003; 85: 126.
39. Deng CJ, Yao QQ, Feng C, et al. 3D printing of bilineage constructive biomaterials for bone and cartilage regeneration. Adv Funct Mater. 2017; 27(36): 1703117.
40. Mao LX, Xia LG, Chang J, et al. The synergistic effects of Sr and Si bioactive ions on osteogenesis, osteoclastogenesis and angiogenesis for osteoporotic bone regeneration. Acta Biomater. 2017; 61: 217-232.
41. Wang WZ, Miao YK, Zhou XJ, et al. Local delivery of BMP-2 from poly(lactic-co-glycolic acid) microspheres incorporated into porous nanofibrous scaffold for bone tissue regeneration. J Biomed Nanotechnol. 2017; 13(11): 1446-1456.
42. Kwon H, Paschos NK, Hu JC, Athanasiou K. Articular cartilage tissue engineering: the role of signaling molecules. Cell Mol Life Sci. 2016; 73: 1173-1194.
43. Wu Y, Zhu S, Wu CT, et al. A bi-lineage conducive scaffold for osteochondral defect regeneration. Adv Funct Mater. 2014; 24 (28): 4473-4483.
44. Zhen GH, Wen CY, Jia XF, et al. Inhibition of TGF-beta signaling in mesenchymal stem cells of subchondral bone attenuates osteoarthritis. Nat Med. 2013; 19 (6):704.
45. Wang TY, Lai JH, Han L, Tong XM, Yang F. Modulating stem cell-chondrocyte interactions for cartilage repair using combinatorial extracellular matrix-containing hydrogels. J Mater Chem B. 2016; 4 (47): 7641-7650.
46. Dahlin RL, Kinard LA, Lam J, et al. Articular chondrocytes and mesenchymal stem cells seeded on biodegradable scaffolds for the repair of cartilage in a rat osteochondral defect model. Biomaterials. 2014; 35 (26): 7460-7469.
47. Hubka KM, Dahlin RL, Meretoja VV, Kasper FK, Mikos AG. Enhancing chondrogenic phenotype for cartilage tissue engineering: monoculture and co-culture of articular chondrocytes and mesenchymal stem cells. Tissue Eng Part B. 2014; 20 (6): 641-654.
48. Zhang FJ, Luo W, Lei GH. Role of HIF-1a and HIF-2a in osteoarthritis. Joint Bone Spine. 2015; 82: 144-147.
49. Duval E, Bauge C, Riamanalijaona R. Molecular mechanism of hypoxia-induced chondrogenesis and its application in in vivo cartilage tissue engineering. Biomaterials. 2012; 33 (26): 6042-6051.
50. Amarilio R, Viukov SV, Sharir A, et al. HIF-1a regulation of SOX9 is necessary to maintain differentiation of hypoxic prechondrogenic cells during early skeletogenesis. Development. 2007; 21 (134): 3917-3928.
51. Yang S, Kim J, Ryu JH. et al. Hypoxia-inducible factor-2a is a catabolic regulator of osteoarthritic cartilage destruction. Nat Med. 2010; 16: 687-693.
52. Hirata M, Kugimiya F, Fukai A. C/EBP beta and RUNX2 cooperate to degrade cartilage with MMP-13 as the target and HIF-2 alpha as the inducer in chondrocytes. Hum Mol Genet. 2012; 21(5): 1111-1123.
53. Vincenti MP, Brinckerhoff CE. Transcriptional regulation of collagenase (MMP-1, MMP-13) genes in arthritis: integration of complex signaling pathways for the recruitment of gene-specific transcription factors. Arthritis Res. 2002; 4: 157-164.
54. Stanton H, Rogerson FM, East CJ, et al. ADAMTS5 is the major aggrecanase in mouse cartilage in vivo and in vitro. Nature. 2005; 434 (7033): 648-652.
55. Huang K, Wu L. Aggrecanase and aggrecan degradation in osteoarthritis: a review. J Int Med Res. 2008; 36 (6), 1149-1160.
56. Ryu JH, Lee A, Huh MS, et al. Measurement of MMP activity in synovial fluid in cases of osteoarthritis and acute inflammatory conditions of the knee joints using a fluorogenic peptide probe-immobilized diagnostic kit. Theranostics. 2012; 2 (2):198-206.

57. Poulet B, Liu K, Plumb D, et al. Overexpression of TIMP-3 in chondrocytes produces transient reduction in growth plate length but permanently reduces adult bone quality and quantity. PLoS One. 2016; 11(12): 0167971.
58. Li W, Wu MJ, Jiang SJ, et al. Expression of ADAMTS-5 and TIMP-3 in the condylar cartilage of rats induced by experimentally created osteoarthritis. Archives of Oral Biology. 2014; 59: 524-529.
59. Lim NH, Kashiwagi M, Visse R. Reactive-site mutants of N-TIMP-3 that selectively inhibit ADAMTS-4 and ADAMTS-5: biological and structural implications. Biochem J. 2010; 431: 113-122.